ILLOC: In-Hall Localization with Standard LoRaWAN Uplink Frames

DONGFANG GUO, Nanyang Technological University, Singapore
CHAOJIE GU*, Zhejiang University, China
LINSHAN JIANG, Nanyang Technological University, Singapore
WENJIE LUO, Nanyang Technological University, Singapore
RUI TAN, Nanyang Technological University, Singapore

LoRaWAN is a narrowband wireless technology for ubiquitous connectivity. For various applications, it is desirable to localize LoRaWAN devices based on their uplink frames that convey application data. This localization service operates in an unobtrusive manner, in that it requires no special software instrumentation to the LoRaWAN devices. This paper investigates the feasibility of unobtrusive localization for LoRaWAN devices in hall-size indoor spaces like warehouses, airport terminals, sports centers, museum halls, etc. We study the TDoA-based approach, which needs to address two challenges of poor timing performance of LoRaWAN narrowband signal and nanosecond-level clock synchronization among anchors. We propose the ILLOC system featuring two LoRaWAN-specific techniques: (1) the cross-correlation among the differential phase sequences received by two anchors to estimate TDoA and (2) the just-in-time synchronization enabled by a specially deployed LoRaWAN end device providing time reference upon detecting a target device's transmission. In a long tunnel corridor, a $70 \times 32\,\text{m}^2$ sports hall, and a $110 \times 70\,\text{m}^2$ indoor plaza with extensive non-line-of-sight propagation paths, ILLOC achieves median localization errors of 6 m (with 2 anchors), 8.36 m (with 6 anchors), and 15.16 m (with 6 anchors and frame fusion), respectively. The achieved accuracy makes ILLOC useful for applications including zone-level asset tracking, misplacement detection, airport trolley management, and cybersecurity enforcement like detecting impersonation attacks launched by remote radios.

CCS Concepts: • **Networks** → **Location based services**; *Wireless access points, base stations and infrastructure*; • **Computer systems organization** → *Sensor networks*.

Additional Key Words and Phrases: LoRaWAN, indoor localization, TDoA

---

*Part of this work was completed while Chaojie Gu was with Nanyang Technological University, Singapore.

Authors' addresses: Dongfang Guo, School of Computer Science and Engineering, Nanyang Technological University, Block N4, B2a-01, 50 Nanyang Avenue, Singapore, 639798, dongfang.guo@ntu.edu.sg; Chaojie Gu, College of Control Science and Engineering, Zhejiang University, 38 Zheda Road, Hangzhou, Zhejiang, China, 310027, gucj@zju.edu.cn; Linshan Jiang, School of Computer Science and Engineering, Nanyang Technological University, Block N4, B2a-01, 50 Nanyang Avenue, Singapore, 639798, linshan001@e.ntu.edu.sg; Wenjie Luo, School of Computer Science and Engineering, Nanyang Technological University, Block N4, B2a-01, 50 Nanyang Avenue, Singapore, 639798, wenjie005@e.ntu.edu.sg; Rui Tan, School of Computer Science and Engineering, Nanyang Technological University, Block N4, 02c-85, 50 Nanyang Avenue, Singapore, 639798, tanrui@ntu.edu.sg.

---

1 INTRODUCTION

Low-power wide-area networking (LPWAN) is a wireless access network paradigm that provides narrowband connectivity to the Internet of Things (IoT) objects distributed in a geographic area. LPWAN systems follow the star topology, in which each *end device* communicates with the *gateway(s)* in one hop. Among various LPWAN technologies (including NB-IoT and Sigfox), LoRaWAN, which is an open data link layer specification based on the LoRa physical layer technique, offers the advantages of using license-free industrial, scientific and medical (ISM) frequency bands, low costs for end devices, and independence from managed infrastructures. Thus, LoRaWAN has been favorably considered for IoT systems [53]. LoRaWAN signals have also been exploited for ubiquitous sensing tasks including human respiration sensing and human walking monitoring [69, 70].

While LoRaWAN is mainly designed for establishing connectivity, being able to localize LoRaWAN devices unobtrusively using their uplink frames is desirable. Note that wireless device localization is one of the ubiquitous computing tasks [17, 29, 55, 66]. The unobtrusiveness here means that no special software instrumentation is needed for the LoRaWAN end devices. As such, the localization service is free from entanglement with any other applications running on the LoRaWAN devices; the already deployed LoRaWANs can develop the localization capability seamlessly. Most existing LoRaWAN localization systems are for outdoor environments (cf. Section 2). The SateLoc [35] and OwLL [8] are two representatives based on received signal strength indicator (RSSI) and time difference of arrival (TDoA), respectively. By considering the impact of outdoor land-cover type on path loss and using satellite images for identifying land-cover types, SateLoc achieves a median error of 47.1 m. OwLL adopts TDoA-based multilateration and applies frequency stitching to overcome LoRaWAN's narrowband challenge. By using both TV whitespace and ISM bands, OwLL in an outdoor deployment achieves 15.7 m median error for non-line-of-sight (NLOS) locations and 9 m median error across line-of-sight (LOS) and NLOS locations. However, the use of TV whitespaces is beyond the LoRaWAN specification [37]. OwLL requires the end device to support TV whitespaces and software instrumentation to implement frequency hopping.

Differently, we quest unobtrusive localization for LoRaWAN devices in indoor environments. We focus on *hall-size* two-dimensional (2D) indoor spaces. Examples of such indoor spaces include expo centers, warehouses, museum halls, single-storey supermarkets, airport terminals, etc. In such environments, Wi-Fi and Bluetooth-based device localization solutions have been available. However, these solutions have respective issues to be managed. Wi-Fi is power-intensive and ill-suited for energy-constrained IoT objects. Although Bluetooth can achieve tens of meters communication ranges, our tests using Feasycom FCS-BP103B Bluetooth beacons show that the functional range for ranging is within 15 m to maintain sub-5 m accuracy. When the actual distance is more than 15 m, the ranging error increases drastically. These results are consistent with those in [11]. Thus, dense Bluetooth beacon deployment is in general required. Owing to above, in this paper, we aim at investigating the attainable accuracy in localizing in-hall end devices using standard LoRaWAN uplink frames.

This paper presents the design and evaluation of a TDoA-based, unobtrusive in-hall LoRaWAN localization (ILLOC) system for any off-the-shelf LoRaWAN end devices. ILLOC deploys multiple *anchors* with known positions and estimates the position of an end device based on the anchors' TDoA measurements regarding any single uplink frame from the end device. The anchors are based on software-defined radios (SDRs) to access the physical layer. We prototype ILLOC using both Universal Software Radio Peripheral (USRP) and LimeSDR that is about 10x cheaper than USRP as the anchor. The design of ILLOC faces the following two challenges:

Challenge 1: Narrowband. To estimate TDoA, a signal that is short in time domain and spreads over a wide frequency band is desirable. For instance, the ultra-wideband (UWB) radio that is designed for precise ranging can transmit a 2 ns impulse signal spreading over a 500 MHz frequency band. However, LoRa's Chirp Spread Spectrum (CSS) modulation uses narrow frequency bands (125 to 500 kHz). Thus, LoRa signals are long and smooth in time domain. Determining the arrival time of a LoRa signal for the purpose of ranging and localization

is challenging. Without special treatment, the uncertainty of estimating the arrival time of a transmission with 125 kHz bandwidth is up to 8 μs, which is translated to 2.4 km distance in ranging [8].

Challenge 2: Inter-anchor clock skews. Tight synchronization of the anchors' clocks (ideally, to nanoseconds accuracy) is a basis of TDoA-based multilateration. However, implementing highly accurate clock synchronization can incur large deployment overhead. For an in-hall LoRaWAN, a specially engineered wired network (e.g., IEEE-1588 network) interconnecting the anchors can achieve nanoseconds synchronization accuracy, but incurs cabling work and thus increased deployment costs. The best civil Global Positioning System (GPS) receivers can provide global time with tens of nanoseconds accuracy. However, for good satellite signal reception, the GPS antennas need to be installed outdoors, also incurring cabling work to connect to the indoor anchors.

To address the above technical challenges, we make the following designs:

Differential phase sampling (DPS). Both USRP and LimeSDR can sample the baseband signal at 25 Msps with an interval of 40 ns. The 40 ns time is translated to 12 m in ranging. To avoid loss of time resolution, ILLOC applies the cross-correlation maximization technique on two 25 Msps signals received by two anchors to determine TDoA. Operating on the signals over a sufficiently long time duration, the cross-correlation maximization assists combating with the narrowband challenge. However, the phase of the raw CSS signal sampled by the SDR contains the phase of the SDR's locally generated reference carrier, which is unknown. To remove the effect of the unknown local phase, we propose a novel DPS scheme that transforms the raw CSS signal to a sequence of the phase differences between any two consecutive CSS samples. The TDoA obtained from the cross-correlation maximization on the DPS traces is not affected by the unknown phases of the local reference carriers.

Just-in-time (JIT) synchronization. Instead of maintaining tight clock synchronization among the anchors' clocks at all times, we implement a *resonator* with an end device hardware and deploy it at a known position. The resonator uses LoRa's Channel Activity Detection (CAD) feature [15] to continuously monitor the channel activities. Once an uplink transmission is detected, the resonator transmits another uplink frame using a different frequency channel. Based on the known distance between the resonator and each anchor as well as the anchors' unsynchronized TDoA measurements, the instantaneous clock skews among the anchors can be identified. With this JIT synchronization, we are no longer entangled with the issue of anchors' clock drifts.

We have implemented ILLOC and evaluated it in several indoor environments. In a long tunnel corridor with two anchors, ILLOC achieves a median 1D localization error of 6 m. In a $70 \times 32\,\text{m}^2$ sports hall with six anchors, ILLOC achieves a median 2D localization error of 8.36 m. In a $110 \times 70\,\text{m}^2$ indoor plaza, where 62% paths are NLOS, ILLOC achieves a median 2D localization error of 15.16 m with six anchors. Thus, ILLOC achieves a similar accuracy as the localization system OwLL [8] that is evaluated outdoor and uses much more frequency spectrum resources. Although the localization accuracy achieved by ILLOC is less exciting compared with sub-meter accuracy, ILLOC's unobtrusive localization service can be useful for numerous scenarios. For instance, in a warehouse, 10m-level localization accuracy is useful for zone-level asset tracking, misplacement detection, etc. In supermarkets and airports, LPWAN radios have been used for trolley management [10, 51], where trolleys' coarse location information is useful. The 10m-level localization can be also used to detect impersonation and replay attacks launched from a malicious radio far away from the victim LoRaWAN end device [19].

The main contributions of this paper are summarized as follows:

- We propose DPS to address the timing challenges arising from the narrowband nature of LoRa.
- We use DPS and LoRa's CAD to realize JIT synchronization and attain the accuracy needed by localization.
- ILLOC achieves sub-10 m median localization accuracy in relatively clean indoor environments and about 15 m accuracy in a complex indoor environment with extensive NLOS paths.

The rest of this paper is organized as follows. Section 2 reviews preliminaries and related work. Section 3 and Section 4 present the overall and detailed system designs. Section 5 presents system implementation. Section 6 presents evaluation results. Section 7 discusses relevant issues and limitations. Section 8 concludes this paper.

(a) Two chirps under LoRa's CSS modulation with SF=1
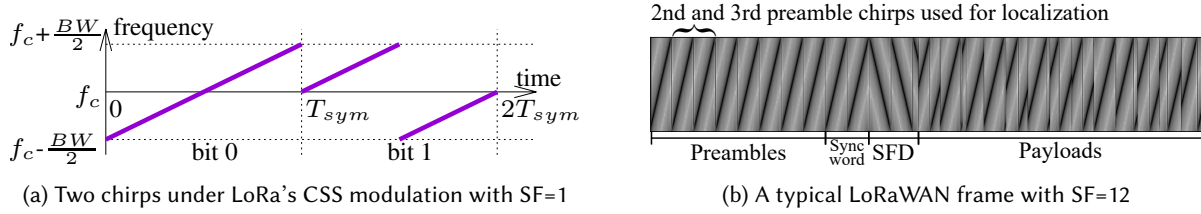
(b) A typical LoRaWAN frame with SF=12

Fig. 1. Spectrograms of LoRa chirps and a LoRa frame.

2 BACKGROUND AND RELATED WORK

This section presents a primer of LoRa and LoRaWAN (Section 2.1), then reviews the related work (Section 2.2).

2.1 A Primer of LoRa and LoRaWAN

LoRa is the physical layer used by LoRaWAN. The ISM frequency band used by LoRa is divided into multiple channels. An end device can select a channel for data communications. LoRa adopts CSS modulation, in which each chirp sweeps the whole bandwidth (BW) of the used channel linearly with time. Given a spreading factor (SF), LoRa evenly divides the BW into 2^{SF} bins as the starting points for chirps to represent 2^{SF} symbols. Fig. 1a illustrates the two symbols when SF = 1 and the central frequency is f_c. We use SF = 1 for illustration only; in practice, LoRa supports six SF settings from 7 to 12. In Fig. 1a, the starting frequencies of the two chirps are $f_c - \frac{\text{BW}}{2}$ and f_c, respectively. When a chirp reaches the bound of BW, it wraps around and continues sweeping the BW until reaching its starting frequency. We call the chirps with positive gradient *up chirps* and those with negative gradient *down chirps*. The symbol time, denoted by T_{sym}, is given by $\frac{2^{\text{SF}}}{\text{BW}}$.

LoRaWAN is a data link layer specification. Fig. 1b shows a typical LoRaWAN frame with three parts: a preamble of eight up chirps, a sync word of two up chirps, a Start Frame Delimiter (SFD) of $2\frac{1}{4}$ down chirps, and a payload of multiple data chirps. LoRaWAN defines three classes (A, B, C) that have different features to meet application needs. Class A is the default, in which all communications are initiated by end devices. Class B additionally uses the gateway to broadcast synchronization beacons. Class C end device keeps listening for downlink frames. ILLOC is compatible with all classes, because ILLOC performs localization with any uplink frame.

2.2 Related Work

2.2.1 LPWAN Localization. Existing studies on localizing LPWAN end devices can be divided into four categories: path loss model-based, location fingerprinting with received signal strength indicator (RSSI), TDoA-based, and angle of arrival (AoA)-based. They are reviewed in this section and summarized in Table 1.

Path loss model-based. In [30], the RSSI measurements collected from a $120 \times 50\,\text{m}^2$ outdoor area fit well into the log-distance path loss model. It achieves a mean localization error of 11.2 m. However, the environment in [30] is relatively simplistic. The study [31] proposes various techniques to reduce the impact of Gaussian and non-Gaussian noises in RSSI measurements on the path loss model-based localization. With six to eight anchors, the average localization errors of the various variants of the proposed approach are within $[20\,\text{m}, 40\,\text{m}]$ and $[10\,\text{m}, 20\,\text{m}]$ in two outdoor spaces with dimensions of $110 \times 64\,\text{m}^2$ and $90 \times 82\,\text{m}^2$, respectively. In a semi-outdoor space with dimension of $36 \times 11\,\text{m}^2$, the average localization errors are within $[10\,\text{m}, 270\,\text{m}]$. The SateLoc system [35] considers the impact of land-cover types on the path loss model. It achieves a median localization error of 47.1 m in a $650 \times 350\,\text{m}^2$ urban area. From [31, 35], the accuracy of outdoor LoRa localization based on path loss models is in general tens of meters and is affected by the distances between the end device and the anchors. The

Table 1. Comparison of approaches for localizing off-the-shelf LPWAN end devices.

Category	Ref.	Radio	Environment	Evaluation Area	# of anchors	# of target positions	Error
Path loss model with RSSI			outdoor	$110 \times 64\,\text{m}^2$	6	3	mean: [20 m, 40 m]
	[31]	LoRa	outdoor	$90 \times 82\,\text{m}^2$	8	6	mean: [10 m, 20 m]
			semi-outdoor	$36 \times 11\,\text{m}^2$	6	3	mean: [10 m, 270 m]
	[35]	LoRa	outdoor	$650 \times 350\,\text{m}^2$	3	38	median: 47.1 m
	[30]	LoRa	outdoor	$120 \times 50\,\text{m}^2$	6	n/a	mean: 11.2 m[†]
	[21]	LoRa	indoor	$25 \times 23\,\text{m}^2$	1	n/a	3.72 m for ranging[†]
Location fingerprinting with RSSI*	[4]	LoRa	outdoor	$10 \times 6\,\text{km}^2$	68	n/a	mean: 398.4 m
	[49]	Sigfox	outdoor	n/a	2/3	18	90th percentile: 50m
	[20]	LoRa	in/outdoor	$150 \times 250\,\text{m}^2$	10	n/a	RMS: 20-30 m
	[46]	LoRa	outdoor	$10 \times 6\,\text{km}^2$	68	n/a	mean: 191.5 m
			indoor	$28 \times 8\,\text{m}^2$	2	n/a	mean: 1.3 m**
	[54]	LoRa	indoor	$104 \times 26\,\text{m}^2$	2	17	96.72% accuracy
	[44]	LoRa	indoor	n/a	1	4	98% accuracy
	[71]	LoRa	indoor	$50 \times 100\,\text{m}^2$	3-4	100+	sub-10 m**
TDoA-based	[50]	LoRa	outdoor	n/a	n/a	n/a	around 100 m
	[14]	LoRa	outdoor	$2 \times 3\,\text{km}^2$	4	3	around 100 m
	[45]	LoRa	outdoor	n/a	3 or more	1648	median: 200 m
	[7]	LoRa	outdoor	n/a	5	4	mean: ≤ 100 m
	[8][‡]	LoRa	outdoor	$300 \times 220\,\text{m}^2$	8	50	median: 9 m
							15.7 m with NLOS
	ILLOC	LoRa	indoor	$70 \times 32\,\text{m}^2$	6	18	median: 8.36 m
				$110 \times 70\,\text{m}^2$	6	14	15.16 m with NLOS
AoA-based	[36][‡]	LoRa	outdoor	$100 \times 60\,\text{m}^2$	4	27	median: 4.4 m
			indoor	$25 \times 15\,\text{m}^2$	4	33	median: 2.4 m with NLOS

*Location fingerprinting approach requires a laborious process of fingerprinting many/all locations.

**The error level depends on the spatial density of the location fingerprints and classification accuracy.

[†]The testing environments might be well controlled such that RSSI measurements match the log-distance path loss model very well, which are inconsistent with our measurements as shown in Section 3.1.

[‡]The systems in [8] and [36] require predefined frequency hopping, and [8] requires using TV whitespaces, whereas ILLOC uses standard LoRaWAN. Table 2 presents a detailed comparison.

work [21] reports an attempt of indoor LoRa localization. It shows that LoRa outperforms Wi-Fi and Bluetooth in terms of the temporal stability of RSSI. However, as shown by our measurements in Section 3.1, the reflections and attenuation caused by walls and barriers present significant challenges to modeling path losses. The large localization errors up to hundreds meters obtained semi-outdoor in [31] echo this challenge.

Location fingerprinting with RSSI. This category of approaches matches the RSSI measurements regarding an end device with those collected offline at known positions (i.e., location fingerprints) to determine the location of the end device at run time. Various machine learning algorithms such as k-nearest neighbors (k-NN) [4, 54], support vector machines (SVM) [49], Gaussian process [20], Bernoulli process [71], and artificial neural networks (ANN) [44, 46] have been used to implement the matching. The work [4] achieves a mean localization error of about 400 m in urban areas. The work [54] achieves a location recognition accuracy of 96.72% indoor. The studies [20, 49] achieve localization errors of tens of meters. The study [46] uses ANN on both an outdoor dataset [4] and a small-scale indoor testbed, achieving mean errors of 191.5 m and 1.27 m, respectively. The work [44] leverages the frequency diversity and achieves a 98% classification accuracy among four positions indoor. A recent

Table 2. Comparison among OwLL [8], Seirios [36] and ILLOC.

Features	OwLL [8]	Seirios [36]	ILLOC
Category	TDoA-based	AoA-based	TDoA-based
Environment	outdoor	in/outdoor	indoor
Evaluation area	$300 \times 220\,\text{m}^2$	$100 \times 60\,\text{m}^2$ (outdoor) $25 \times 15\,\text{m}^2$ (indoor)	$70 \times 32\,\text{m}^2$ $110 \times 70\,\text{m}^2$
# of anchors	8 (4 for sync)	4	6
Synchronization	via 4 anchors	interchannel	via 1 resonator
Spectrum usage	400 MHz	1.6 MHz	250 kHz
Frames per query	80 to 120	8	1 or more
Unobtrusive?	No*	No†	Yes
Error	median: 9 m 15.7m w/ NLOS	median: 4.4 m (outdoor) 2.4 m (indoor w/ NLOS)	median: 8.36 m 15.16m w/ NLOS

*OwLL requires end device to support TV whitespaces and software instrumentation for frequency hopping.

†Seirios requires software instrumentation for frequency hopping.

work [71] defines extreme RSS (ERSS) to obtain more stable RSS fingerprints and achieves sub-10 m accuracy indoor. However, these approaches [4, 20, 49, 71] require a laborious blanket process of fingerprinting many/all locations, which presents a high deployment overhead. In addition, as evaluated in Section 3.1, the learning-based approaches [44, 46, 49, 54, 71] are subject to the fingerprint model aging issue.

TDoA-based: Several studies [7, 14, 45, 50] have attempted the TDoA-based approach to localize LoRa end devices. For instance, Semtech [50] uses Global Navigation Satellite System (GNSS)-synchronized commodity gateways to perform outdoor TDoA-based localization. The solution achieves a median error of around 100 m by combining the results of 128 frames. These TDoA methods rely on the timestamps of frame arrival given by commodity gateways, which in general have microsecond granularity. Such coarse-grained timestamps cannot support accurate ranging and localization. Therefore, their localization errors are tens to hundreds of meters, which are consistent with the microsecond granularity of timestamps. The OwLL system [8] achieves a median error of 9 m over a $300 \times 220\,\text{m}^2$ outdoor area based on TDoA. It includes TV whitespaces for frequency hopping to make a wideband illusion. As an attempt of exploiting TV whitespaces that are beyond the LoRaWAN specification, it needs to ensure the compliance with the geo-dependent TV whitespace policies, including detailed issues such as whether each end device needs to check the shared databases of available TV whitespace channels [8]. Besides, OwLL needs to send 80 to 100 frames per localization query to cover the 400 MHz wideband, which introduce extra time and energy overhead. Differently, ILLOC is based on standard LoRaWAN uplink frames in the ISM bands. ILLOC only needs one frame for prompt one-shot localization. Thus, while ILLOC and OwLL achieve similar accuracy, ILLOC imposes fewer requirements and overheads.

AoA-based: The Seirios system [36] studies AoA for LoRaWAN device localization. In Seirios, two antennas are mounted on each SDR-based anchor. Seirios exploits the physical layer structure of LoRa signals to synchronize them in multiple channels. The synchronized channel state information (CSI) features are then used by the super-resolution algorithm to resolve the multipaths and locate the device. Seirios achieves median errors of 4.4 m and 2.4 m over a $100 \times 60\,\text{m}^2$ outdoor area and a $25 \times 10\,\text{m}^2$ indoor area, respectively. Similar to OwLL, the end device in Seirios needs to transmit in a predefined frequency-hopping manner over eight LoRaWAN channels per localization query. Thus, Seirios needs special software instrumentation at the end devices.

Table 2 summarizes the comparison between OwLL, Seirios, and ILLOC.

Table 3. Comparison of indoor localization technologies.

Signal	Low power?	Functional range[*]	Error
Wi-Fi [5, 25, 26, 47, 64]	✗	< 30 m	< 0.9 m
Bluetooth [6, 11, 33]	✓	< 15 m	≈ 1 m
Cellular [27, 43, 48]	✗	≈ 35-60 m	≈ 0.8 m
RFID [22, 59, 60, 65]	✓	< 6 m	< 0.1 m
UWB [12, 18, 58]	✓	< 50 m	≈ 0.1 m
Zigbee [9, 52, 56]	✓	< 20 m	≈ 1-2 m
Visible light [28, 34, 62, 63, 68]	✓/✗[†]	in a room[‡]	≈ 0.1 m
RF backscatter [38, 41, 57]	✓	tens of m	< 0.5 m
LoRaWAN (ILLOC)	✓	≈ 110 m	≈ 8-15 m

[*]Functional range for accuracy in the next column. It is not the communication range.

[†]Depends on the type of target nodes.   [‡]Visible light localization systems cannot work in NLOS scenarios.

As shown in Table 1, most existing works focus on outdoor environments. Differently, we investigate the feasibility of localizing LoRaWAN end devices in large hall-size indoor environments. The existing TDoA-based approaches [7, 14, 45] use commodity gateways as the anchors, which, however, cannot achieve satisfactory localization accuracy due to the gateways' microsecond timestamping granularity. ILLOC and the recent OwLL, Seirios employ SDR-based anchors in similar quantities to achieve (sub) 10 m-level localization accuracy. ILLOC uses standard LoRaWAN frames and is unobtrusive; Seirios needs special software instrumentation at the end device; OwLL needs both hardware support for TV whitespaces and software instrumentation at the end device.

2.2.2 Broader Solutions for Indoor Localization. Beyond LPWAN end device localization, there is a body of literature on indoor localization based on radio frequency (RF) and other signals. The survey [61] divides the existing solutions into device-based and device-free categories. ILLOC is device-based. The work [13] includes a brief summary of the existing RF-based solutions based on their requirements of (1) dedicated infrastructure for providing localization signals, (2) training process to collect data for subsequent localization, and (3) additional equipment for end devices. Most existing technologies do not have all three requirements, but at least one [13]. ILLOC requires the installation of an infrastructure (i.e., the anchors and resonator). The cost of an anchor can be down to about 100 US$, similar to a commodity LoRaWAN gateway (see the cost analysis in Section 7). The deployment overhead is the determination of the anchor and resonator locations, which is a one-time effort and a common prerequisite for TDoA approaches. Thus, the cost and overhead for setting up ILLOC for an existing LoRaWAN are low. In Section 7, we will discuss the suitable application scenarios of ILLOC, after evaluating its accuracy in various real environments. Table 3 presents a high-level comparison among various indoor localization technologies in terms of power consumption, localization range and accuracy. While some technologies achieve good localization accuracy in certain scenarios, there are still no solutions good for all environments and settings. Most existing solutions cannot be simultaneously low-power, long-range (up to 100 m), and accurate. This paper aims to explore the indoor localization capability for existing LoRaWAN devices in indoor environments simply with their standard uplink frames. With ILLOC, the already deployed indoor LoRaWAN devices can be localized without any modification and still function in a low-power and long-range manner.
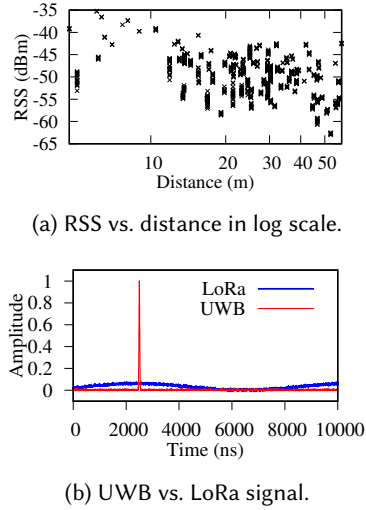
(a) RSS vs. distance in log scale.

(b) UWB vs. LoRa signal.

Fig. 2. Data illustrating the challenges of indoor LoRa localization.
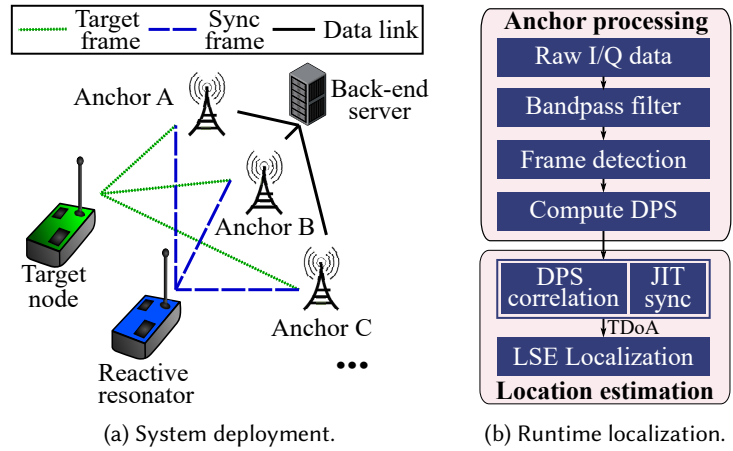

(a) System deployment.

(b) Runtime localization.

Fig. 3. ILLOC: Unobtrusive in-hall LoRaWAN localization system.

3 MOTIVATION AND OVERVIEW OF ILLOC

3.1 Challenges of Indoor LoRa Localization

This section discusses the challenges faced by the three categories of approaches (cf. Table 1) in indoor settings.

We measure LoRa RSS in an indoor sports hall sized $70 \times 32\,\mathrm{m}^2$, which is an evaluation space used in this paper with details presented in Section 6. Specifically, we carry a LoRaWAN end device to 18 grid points in the sports hall and compute the RSS at six distributed anchors. Fig. 2a shows a scatter plot of the RSS in decibel versus the distance between the end device and anchor in a $\log_{10}$ scale. From the widely adopted log-distance path loss model, ideally, the measurements in Fig. 2a should follow a linear trend. The linear fitting with the measurements shown in Fig. 2a yields a R^2 score of 0.28 only. If we use the fitted log-distance path loss model to perform ranging, the median ranging error is 1.3 km. This implies that the path loss model-based approach will have low performance in indoor environments. A possible reason is that the stronger multi-path effects in the indoor environment render the log-distance path loss model inaccurate.

We collect RSS fingerprints on 14 positions in a $110 \times 70\,\mathrm{m}^2$ indoor plaza, which is another evaluation space used in this paper, and revisit these positions to collect data after two months. (Fig. 10b shows the 14 positions.) We implement five RSS fingerprinting approaches based on SVM [49], k-NN [54], ANN [46], ANN with frequency diveristy [44], and ERSS [71]. Note that the approach [44] exploits frequency diversity and uses a non-standard frequency hopping approach. For a fair comparison, we replace its frequency hopping mechanism with LoRaWAN-compliant random hopping. For all five approaches, six anchors are used to record the RSS fingerprints. When the training and testing data are split from the same round of data collection, these five approaches achieve 100% classification accuracy. However, when the models are trained with the data in the first-round data collection and tested with the second-round data collection two months later, the position recall accuracy drops to 30.93%, 31.71%, 42.1%, 43.90%, and 30.99%, respectively. Besides, we also conduct a 30-day consecutive study with 16 static LoRaWAN end devices and three gateways in a $27 \times 17\,\mathrm{m}^2$ office. Trained with the first-day data and tested with other remaining 29 days' data, the classification accuracy drops from above 90% on day 2 to less than 60%

after 24 days. These results show the fingerprint model aging issue that can be caused by the gradual changes of RF environment [67]. Thus, it is necessary to frequently fingerprint all locations.

For TDoA-based approaches, measuring the time of arrival (ToA) of LoRa signal is challenging due to the signal's narrowband nature and the resulting smooth time-domain characteristics. Fig. 2b contrasts the time-domain features of LoRa and UWB. A UWB impulse concentrates its energy within a few nanoseconds, which enables accurate determination of ToA. However, the waveform of LoRa changes slowly with time. It is difficult to tell the precise timing of the signal arrival. Note that the presented duration of 10,000 ns in Fig. 2b is merely 1% of a LoRa symbol duration (SF = 7, BW = 125 kHz). To achieve accurate timing for LoRa signals, ILLOC captures LoRa's CSS pattern accumulated in the time domain to deal with the narrowband challenge.

3.2 Deployment of ILLOC

Fig. 3a illustrates the setup of ILLOC. It deploys at least three *anchors* at known positions. When more anchors are deployed, the localization accuracy can be improved. Each anchor is equipped with an SDR that samples the baseband signal at a rate high enough to provide good time granularity. All anchors are connected to a *back-end server* via data links. At run time, each anchor processes the baseband signal of the uplink frame and transmits the result to the back-end server. Then, the back-end server estimates the location of the end device.

The end device to be localized is called *target node*. It uses an off-the-shelf LoRaWAN radio. If only the infrastructure needs to know the location of the target node, no special software programs are needed at the target node – it will be localized once it transmits any uplink frame. If the target node needs to know the localization result, the LoRaWAN gateway can include the result in the downlink frame to the target node. For instance, in Class A LoRaWAN, there are two subsequent downlink windows after an uplink frame [37].

To achieve tight clock synchronization among the anchors upon an uplink frame, we deploy a *resonator*, which is a normal off-the-shelf LoRa end device loaded with our program. The resonator continuously monitors the channel activities and transmits a *sync frame* once upon it detects an uplink frame transmission from any target node. When there are many target nodes in the field, this resonator may need to transmit sync frames frequently. Section 7 discusses how to reduce the sync frame transmissions. The resonator's position can be chosen such that all anchors have satisfactory RSSIs for the sync frames. The resonator's position is configured to ILLOC.

3.3 Localization Workflow of ILLOC

Fig. 3b presents the localization workflow of ILLOC, which consists of two steps, i.e., *anchor processing* performed by the individual anchors and *location estimation* performed by the back-end server. In what follows, we present the resonator's operations and the overview of the above two steps.

3.3.1 Resonator's Operations for JIT Synchronization. The study [40] proposed an anchor synchronization scheme by using a particular LoRaWAN node that transmits a synchronization frame every few seconds at a fixed, known position to provide time reference. Differently, ILLOC utilizes LoRa's Channel Activity Detection (CAD) feature and multi-channel characteristics to provide a more flexible and timely synchronization across anchors. In ILLOC, the target node and the resonator use two different frequency channels, referred to as *target channel* and *sync channel*, respectively. At run time, the resonator keeps performing CAD on the target channel. CAD is a feature recently included to the LoRaWAN specification to detect preambles when specified with the frequency channel and SF. It is available on all of the latest LoRa radios (e.g., SX126x and SX127x). The duration of a CAD operation is merely $T_{\text{sym}} + \frac{32}{BW}$. With BW = 125 kHz and SF = 12, the CAD just takes 33 ms. Thus, the resonator can quickly detect the *target frame* from some target node. Upon the detection, it immediately transmits a *sync frame* using the sync channel to provide a reference signal to all anchors for JIT synchronization.

Two factors may affect the effectiveness of the sync frame as a reference. First, the sync frame takes different propagation times to arrive at the anchors because of the different distances from the resonator to the anchors.
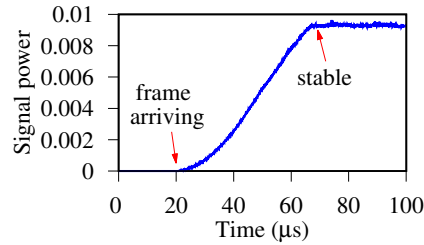
Fig. 4. Received signal power when a LoRaWAN frame arrives at the anchor.

As the propagation times can be estimated based on the known positions of the anchors and resonator, the propagation times can be accounted for in synchronizing the anchors. Second, since there is a delay in detecting the target frame, which is around a CAD duration, the anchors may develop new clock skews because of their different clock drift rates. Therefore, even if the anchors' clocks are perfectly synchronized at the time instants of receiving the sync frame, the new clock skews projected to the time instants of receiving the target frame remain. There is no effective way to eliminate the new clock skews. However, as the resonator responds quickly via CAD, the anchors' new clock skews during one CAD duration can be safely ignored. For instance, as the oscillator of the SDR we use drifts at a rate of at most 25 ppb, the maximum new clock skew within a CAD duration is merely 0.825 nanoseconds, which is much smaller than the SDR's sample interval of 40 nanoseconds when operating at a 25 Msps sampling rate.

3.3.2 Anchor Processing. The anchor processing step detects the target and sync frames, and then computes the respective DPS sequences. The details are as follows. The anchor applies two band-pass filters on the baseband signal from the SDR to generate two I/Q data streams in the target and sync channels, respectively. As the data processing steps for the two streams are identical, our description focuses on one data stream. The anchor uses an open-source LoRa decoder `gr-lora` [3] to detect the uplink frame in the I/Q data stream. Upon detection, the anchor uses the following procedure to identify the timing of the frame with higher precision. As shown in Fig. 1b, the last up chirp of the sync word and the first down chirp of the SFD form a salient peak pattern in spectrogram. We compute the cross-correlation between this *a priori* pattern and the I/Q data stream. The maximum cross-correlation indicates the timing of the peak (i.e., the start of the SFD). With this timing information, we can locate every chirp of the uplink frame. Note that the accuracy of this timing information is not high enough for TDoA, because the cross-correlation is performed in spectrogram with reduced time resolution.

As discussed in Section 1, we apply the cross-correlation maximization technique on the 25 Msps signals to estimate the TDoA between two anchors. Specifically, the technique slides a signal over another signal and computes the correlation between the two signals at every sliding position; the sliding position with the highest correlation is yielded as the result. However, the I/Q waveform is affected by the unknown phase of the anchor's locally generated carrier for down conversion (cf. Section 4.1.1). As a result, the cross-correlation maximization technique cannot be directly applied on the I/Q waveform. To address this issue, we employ a novel DPS technique that removes the impact of the aforementioned unknown phase.

For the detected frame, the anchor computes a DPS sequence from the I/Q data, and then transmits the DPS sequence to the back-end server for TDoA estimation. Note that we avoid using the first preamble because its signal power can experience a gradual increasing process. Fig. 4 shows this gradual signal power increase of the first preamble chirp of a real transmission. This process lasts for about 50 μs and is due to the receiver's characteristics. Besides, in our preliminary in-lab study presented in Section 6.2.1 on the used pattern length,

two-chirp length has the best correlation accuracy. Therefore, we select the second and the third preamble chirps to compute the DPS sequence.

Each anchor transmits a total of two DPS sequences for the target frame and the sync frame respectively to the back-end server. Note that the DPS sequence is timestamped with the sample indexes in the time domain of the original I/Q data stream before the band-pass filtering. As such, the timestamps of the target frame's and sync frame's DPS sequences are in the same time domain to enable the JIT synchronization at the back-end server. The total volume of the transmitted data by an anchor is less than 30 MB, which can be conveyed in short times using today's local-area networking technologies like 802.11ax and broadband powerline communication. Our tests using 2Gbps TP-Link Powerline show that transmitting an anchor's data over TCP requires 0.8 to 0.9 seconds, shorter than most LoRaWAN frame transmission times of seconds.

3.3.3 Location Estimation. Once the back-end server receives the data from all anchors, it performs following.

JIT synchronization: The back-end server estimates the clock offsets between every two anchors using their DPS sequences corresponding to the sync frame. This is achieved by performing the cross-correlation maximization on the two DPS sequences and also accounting for the sync frame's propagation times to the anchors.

TDoA estimation: For every two anchors, with the estimated clock offset, the back-end server rectifies the timestamps for the two anchors' DPS sequences corresponding to the target frame. Then, the back-end server performs the cross-correlation maximization using the two time-rectified DPS sequences to estimate the TDoA.

Location estimation: The back-end server solves a least square problem that integrates all TDoA estimates and the anchors' known positions to estimate the target node's position.

4 DETAILED DESIGN OF ILLOC

4.1 Differential Phase Sampling (DPS)

Section 4.1.1 models the processes of LoRa chirp signal propagation and SDR's reception to exhibit the issue of unknown reference carrier phases that prevents us from determining the TDoA directly from the raw I/Q traces received by two anchors regarding the same target frame. Section 4.1.2 presents DPS to address the issue.

4.1.1 Modeling LoRa Chirp Signal Propagation and Reception. A chirp is a finite-time signal with time-varying frequency. Denote by t_0 the time instant of starting transmitting a chirp. At time instant t, let $A(t)$ and $f(t)$ denote the instantaneous amplitude and frequency of the chirp signal at the location of the target node. For a preamble up chirp, $f(t)$ is a linear function sweeping the used frequency band over T_{sym}. Let $s(t)$ denote the chirp signal modulated by the target node. From the CSS modulation, we have $s(t) = A(t) \sin\left(2\pi \int_{t_0}^{t} f(x)\mathrm{d}x + \theta_{\text{Tx}}\right)$, where $\theta_{\text{Tx}} \in [0, 2\pi)$ is the target node's initial phase at $t = t_0$. The θ_{Tx} is unknown. As RF signals are transverse waves, the chirp signal at a position d meters from the target node is $s(t, d) = \alpha(d)A\left(t - \frac{d}{c}\right) \sin\left(2\pi \int_{t_0}^{t - \frac{d}{c}} f(x)\mathrm{d}x + \theta_{\text{Tx}}\right)$, where $t \geq \frac{d}{c} + t_0$, $\alpha(d)$ and c denote the attenuation coefficient and the speed of light, respectively.

Now, we model the reception of the LoRa chirp by an SDR d meters from the target node. The SDR generates two unit-amplitude orthogonal carriers $\sin(2\pi f_c t + \theta_{\text{Rx}})$ and $\cos(2\pi f_c t + \theta_{\text{Rx}})$, where f_c is a specified frequency and θ_{Rx} is the initial phase of the two locally generated carriers at $t = 0$. The θ_{Rx} is unknown. The SDR mixes the received signal with the self-generated carriers, yielding $s_I(t, d) = s(t, d) \cdot \sin(2\pi f_c t + \theta_{\text{Rx}})$ and $s_Q(t, d) = s(t, d) \cdot \cos(2\pi f_c t + \theta_{\text{Rx}})$. Then, the SDR applies two internal low-pass filters to remove the high-frequency components in $s_I(t, d)$ and $s_Q(t, d)$. After the low-pass filtering, the I and Q components yielded by the SDR, denoted by $I(t, d)$ and $Q(t, d)$, are given by $I(t, d) = \frac{\alpha(d)A\left(t - \frac{d}{c}\right)}{2} \cos \Theta(t, d)$, $Q(t, d) = \frac{\alpha(d)A\left(t - \frac{d}{c}\right)}{2} \sin \Theta(t, d)$, where $\Theta(t, d) = 2\pi \int_{t_0}^{t - \frac{d}{c}} f(x)\mathrm{d}x - 2\pi f_c t + \theta$ and $\theta = \theta_{\text{Tx}} - \theta_{\text{Rx}}$. The low-pass filtering process can be easily derived

and is thus omitted here due to space constraints. We can see that the waveform of the I/Q trace generated by the SDR depends on both d and θ_{Rx}. Therefore, the task of identifying the TDoA between two anchors directly from the I/Q waveforms is entangled with the unknown phases of their locally generated carriers.

4.1.2 DPS. To disentangle the unknown phases from the problem, we use the sequence of the differences between any two adjacent I/Q data samples. From the above analysis, the instantaneous phase $\Theta(t, d)$ can be computed by $\Theta(t, d) = \text{atan2}(Q(t, d), I(t, d)) + 2k\pi$ where $k \in \mathbb{Z}$. The k rectifies the multi-valued inverse tangent function $\text{atan2}(\cdot, \cdot) \in (-\pi, \pi)$ to an unlimited value domain and ensures that $\Theta(t, d)$ is a continuous function of t. How to determine k will be discussed shortly. Let f_s denote the SDR's sampling rate. Denote by $\{\Theta[t, d], \Theta[t + \frac{1}{f_s}, d], \Theta[t + \frac{2}{f_s}, d], \ldots, \Theta[t + \frac{n}{f_s}, d]\}$ a sequence of instantaneous phases computed by the sampled I and Q values. We define the DPS sequence Δ starting from time t with its ith element $\Delta[i]$ given by $\Delta[i] = \Theta\left[t + \frac{i+1}{f_s}, d\right] - \Theta\left[t + \frac{i}{f_s}, d\right]$. From the model in Section 4.1.1, the analytic expression of $\Delta[i]$ is $\Delta[i] = 2\pi \int_{t + \frac{i}{f_s} - \frac{d}{c}}^{t + \frac{i+1}{f_s} - \frac{d}{c}} f(x) dx - 2\pi f_c \frac{1}{f_s}$. The $\Delta[i]$ is disentangled from θ_{Tx} and θ_{Rx}, and encompasses d. The following proposition solves the issue of determining k for unambiguously computing Δ.

PROPOSITION 1. *$f_s > BW$ is a sufficient condition for computing Δ unambiguously based on the I/Q trace.*

PROOF. First, we analyze the bounds of $\Delta[i]$. The LoRa chirp's instantaneous frequency $f(t) \in \left[f_c - \frac{BW}{2}, f_c + \frac{BW}{2}\right]$. By substituting the $f(x)$ term in the analytic expression of $\Delta[i]$ with its lower bound $(f_c - \frac{BW}{2})$ and upper bound $(f_c + \frac{BW}{2})$, respectivly, we can obtain a lower bound of $\Delta[i]$ as $\Delta[i] \geq 2\pi \int_{t + \frac{i}{f_s} - \frac{d}{c}}^{t + \frac{i+1}{f_s} - \frac{d}{c}} (f_c - \frac{BW}{2}) dx - 2\pi f_c \frac{1}{f_s} = 2\pi (f_c - \frac{BW}{2}) \frac{1}{f_s} - 2\pi f_c \frac{1}{f_s} = -\frac{BW}{f_s}\pi$, and similarly a upper bound as $\Delta[i] \leq \frac{BW}{f_s}\pi$. Thus, we have $-\frac{BW}{f_s}\pi \leq \Delta[i] \leq \frac{BW}{f_s}\pi$. We consider computing a Δ element based on two consecutive Θ values Θ_1 and Θ_2, i.e., $\Delta = \Theta_1 - \Theta_2 = (\text{atan2}(Q_1, I_1) + 2k_1\pi) - (\text{atan2}(Q_2, I_2) + 2k_2\pi) = (\text{atan2}(Q_1, I_1) - (\text{atan2}(Q_2, I_2)) + 2\pi(k_1 - k_2)$, where both k_1 and k_2 are unknown and the term $(k_1 - k_2)$ is to be determined. Since $\Delta \in \left[-\frac{BW}{f_s}\pi, \frac{BW}{f_s}\pi\right]$, with the condition $f_s > BW$ in Proposition 1, the range of Δ must be within $-\pi < \Delta < \pi$. Since $-2\pi < \text{atan2}(Q_1, I_1) - \text{atan2}(Q_2, I_2) < 2\pi$, if $k_1 - k_2 \geq 2$ or $k_1 - k_2 \leq -2$, Δ will be out of its range $(-\pi, \pi)$. Thus, there are only three possible cases: i) $k_1 - k_2 = 1$, ii) $k_1 - k_2 = 0$, and iii) $k_1 - k_2 = -1$. It can be easily verified that there is a case satisfying $\Delta \in (-\pi, \pi)$ and the other two cases must not satisfy $\Delta \in (-\pi, \pi)$. The satisfying case determines the value of $(k_1 - k_2)$. Therefore, the elements of Δ can be determined sequentially without ambiguity. □

Our implemented ILLOC with $f_s = 25\,\text{Msps} \gg BW = 125\,\text{kHz}$ satisfies the condition in Proposition 1. From the proof of Proposition 1, the Δ can be computed as follows. First, compute $\epsilon[i] = \text{atan2}\left(Q\left(t + \frac{i+1}{f_s}\right) / I\left(t + \frac{i+1}{f_s}\right)\right) - \text{atan2}\left(Q\left(t + \frac{i}{f_s}\right) / I\left(t + \frac{i}{f_s}\right)\right)$. If $\epsilon[i] < -\frac{BW}{f_s}\pi$, output $\Delta[i] = \epsilon[i] + \pi$; if $-\frac{BW}{f_s} < \epsilon[i] < \frac{BW}{f_s}\pi$, output $\Delta[i] = \epsilon[i]$; if $\epsilon[i] > \frac{BW}{f_s}\pi$, output $\Delta[i] = \epsilon[i] - \pi$. The top part of Fig. 5a shows the DPS sequence of two real preamble chirps. The DPS sequence of a chirp is linear over time, because the phase of a preamble chirp is a quadratic function of time. A zoomed-in view in Fig. 5a shows that the DPS sequence is subject to random noises.

4.2 TDoA Estimation

This section presents the technique of estimating the TDoA between two anchors regarding the same target frame. In this section, we assume that the clocks of the anchors are synchronized. The details of how to achieve the clock synchronization are presented in Section 4.3. Note that the clock synchronization between the target node and the anchors is not required.
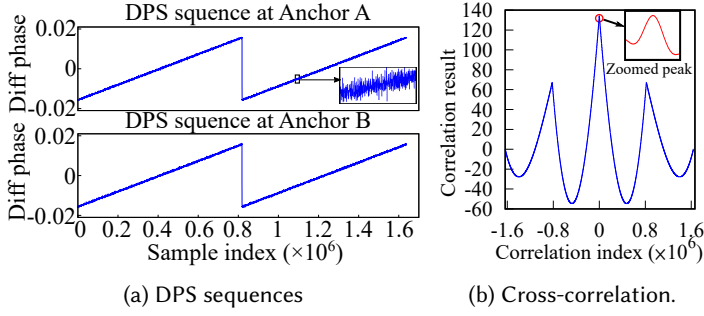
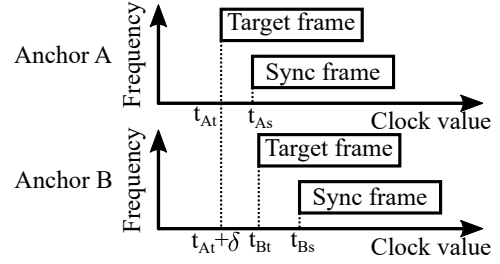Fig. 5. DPS sequences and their cross-correlation.

(a) DPS sequences

(b) Cross-correlation.

Fig. 6. TDoA Calculation with JIT synchronization.

Denote by d_A and d_B the distances from the target node to the anchors A and B, respectively. The DPS sequence on A is Δ_A, where $\Delta_A[i] = 2\pi \int_{t+\frac{i}{f_s}-\frac{d_A}{c}}^{t+\frac{i+1}{f_s}-\frac{d_A}{c}} f(x)dx - 2\pi f_c \frac{1}{f_s}$. Denote by $F(x)$ the antiderivative of $f(x)$. The DPS sequence on A can be expressed as $\Delta_A[i] = 2\pi \left(F\left(t - \frac{d_A}{c} + \frac{i+1}{f_s}\right) - F\left(t - \frac{d_A}{c} + \frac{i}{f_s}\right) \right) - 2\pi f_c \frac{1}{f_s}$. As the variable in this time sequence is $t - \frac{d_A}{c}$, we can denote the sequence as $\Delta_A = S(t - \frac{d_A}{c})$. The DPS sequence on B can be written as $\Delta_B = S(t - \frac{d_B}{c})$. Thus, $\Delta_B = S(t - \frac{d_B}{c}) = S(t - \frac{d_A}{c} + (\frac{d_A}{c} - \frac{d_B}{c}))$. It means that Δ_B is a time-shifted version of Δ_A, where the time shift is $\frac{d_A}{c} - \frac{d_B}{c}$. Hence, we can apply the cross-correlation maximization technique on Δ_A and Δ_B to estimate the time shift. Assuming K is the peak position of the cross-correlation, we have $K \frac{1}{f_s} \approx \frac{d_A}{c} - \frac{d_B}{c}$. As K is an integer, the approximation in the above expression captures the rounding error. Thus, the estimated TDoA is $\text{TDoA}_{AB} = \frac{K}{f_s}$. Fig. 5a shows the DPS sequences computed by two anchors regarding the same real target frame in a controlled experiment where the two anchors are placed at the same position. Fig. 5b shows the cross-correlation between them, in which the peak position is K. Note that we have applied the approach in Section 4.3 to synchronize A and B. Thus, K should be zero in this controlled experiment with zero groundtruth TDoA. Without the synchronization, the K value will contain the clock skew between A and B.

4.3 Just-in-Time (JIT) Synchronization

This section presents the details of using the sync frame from the resonator to achieve JIT synchronization among the anchors. Fig. 6 illustrates the timing of the arrivals of the target/sync frame at two anchors, in which the target node and the resonator are closer to anchor A. Note that the target and sync frames are transmitted in different frequency channels. Consider an unknown clock skew δ between anchor A and anchor B. When A receives the target frame at the time instant t_{At} in terms of A's clock, B's clock value is $t_{At} + \delta$. As such, the TDoA result presented in Section 4.2 contains δ. Specifically, by denoting TDoA_{AB}^t as the actual TDoA regarding the target node and $\widetilde{\text{TDoA}}_{AB}^t$ as the estimated TDoA by the approach presented in Section 4.2 on the unsynchronized DPS sequences, we have $\widetilde{\text{TDoA}}_{AB}^t = \text{TDoA}_{AB}^t + \delta$. Similarly, we apply the cross-correlation maximization technique on the sync frame's DPS sequences. Since the clock skew can be time-varying, for the sync frame, we have $\widetilde{\text{TDoA}}_{AB}^s = \text{TDoA}_{AB}^s + \delta + \delta'$, where δ' is the extra skew during the time period between the arrival time instants of the target and sync frames. From our evaluation in Section 6.2.2, the controlled resonator delay up to two seconds introduce little impact on the TDoA error. Since the CAD delay is just tens of milliseconds as presented in Section 6.2.2, the δ' that is largely introduced during the CAD delay and its impact can be safely ignored. Thus, in our analysis, $\widetilde{\text{TDoA}}_{AB}^s \simeq \text{TDoA}_{AB}^s + \delta$. According to the known positions of the

---

Algorithm 1 Greedy anchor subset fusion algorithm.

Given: Set of anchors $S = \{1, ..., N\}$

Output: $\boldsymbol{p}_{est}$ or one-shot failure

1: $M = N$; solution set $A = \emptyset$;
2: **while** $M \geq 3$ **do**
3:     **for** each subset of M anchors in S **do**
4:         solve the least squares problem with M anchors to $\boldsymbol{p}$; **if** $\boldsymbol{p}$ is in the monitored field **then** $A = A \cup \{\boldsymbol{p}\}$;
5:     **end for**
6:     **if** $A \neq \emptyset$ **then return** geometric median of solutions in A; **otherwise** $M = M - 1$;
7: **end while**
8: **return** one-shot failure

---

two anchors and the resonator, the actual TDoA regarding the sync frame, i.e., TDoA^s_{AB}, is known. Thus, in the presence of clock skew between A and B, the actual TDoA regarding the target node can be computed as $\text{TDoA}^t_{AB} = \widetilde{\text{TDoA}}^t_{AB} - \delta \simeq \widetilde{\text{TDoA}}^t_{AB} - \widetilde{\text{TDoA}}^s_{AB} + \text{TDoA}^s_{AB}$.

4.4 Location Estimation

With the techniques in Sections 4.1-4.3, we have the target frame's TDoA between any two anchors. For any target node's candidate position $\boldsymbol{p}_i$, the analytic TDoA between any two anchors A and B is $\frac{1}{c}\left(\|\boldsymbol{p}_i - \boldsymbol{p}_A\| - \|\boldsymbol{p}_i - \boldsymbol{p}_B\|\right)$, where $\boldsymbol{p}_A$ and $\boldsymbol{p}_B$ are the positions of A and B, respectively. We adopt the least squares approach to estimate the target position as $\boldsymbol{p}_{est} = \text{argmin}_{\forall \boldsymbol{p}_i} \sum_{\substack{\forall A,B \in G}}^{A \neq B} \left(\text{TDoA}^t_{AB} - \frac{1}{c}\left(\|\boldsymbol{p}_i - \boldsymbol{p}_A\| - \|\boldsymbol{p}_i - \boldsymbol{p}_B\|\right)\right)^2$, where TDoA^t_{AB} is the computed TDoA from Section 4.3 and G is the set of used anchors. At least three anchors are needed for 2D localization. When we have N ($N > 3$) anchors, we use a *greedy anchor subset fusion algorithm* as described below to improve the robustness of the location estimation against TDoA outliers. First, we define the one-shot failure and success. In solving the least squares problem, we consider a search area for the candidate position $\boldsymbol{p}_i$ much larger than the monitored field (i.e., the indoor space). If the resulting $\boldsymbol{p}_{est}$ is out of the monitored field, the result is regarded an outlier and the location estimation declares a *one-shot failure*; otherwise, the location estimation declares a *one-shot success*. Then, we describe the algorithm. An iteration of the algorithm considers all subsets of the N anchors where each subset has M anchors, and solves the least squares problem with each anchor subset. The iteration yields the geometric median of the successful one-shot results among the $\binom{N}{M}$ localization trials. When all $\binom{N}{M}$ localization trials fail, the algorithm decreases M by one and proceeds to the next iteration. The algorithm starts from $M = N$ and iterates until $M = 3$. Algorithm 1 shows the pseudocode of the algorithm. From our experiments in a sports hall, this algorithm achieves 100% one-shot success rate and yields similar localization accuracy achieved by using all N anchors during the successful cases.

5 SYSTEM IMPLEMENTATION

Resonator/target node: We use the same hardware for the resonator and the target node. Specifically, we integrate an SX1276-based inAir9B LoRaWAN radio with a 915 MHz antenna and an Arduino Uno microcontroller board powered by a portable power bank. Each end device is placed on a tripod during the experiments. We implement the target frame transmission, resonator's CAD, and sync frame transmission using the open-source Arduino LoRa library `arduino-LoRa` [39]. Transmitting power is set to 20 dBm.

Anchors: We build two types of anchors. The first type is based on USRP N210, a 915 MHz antenna, and an HP Elitebook 830 G6 laptop installed with the USRP's driver and GNU Radio. The laptop performs SDR control,
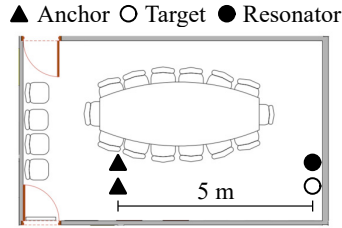
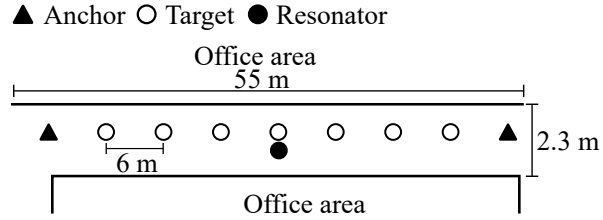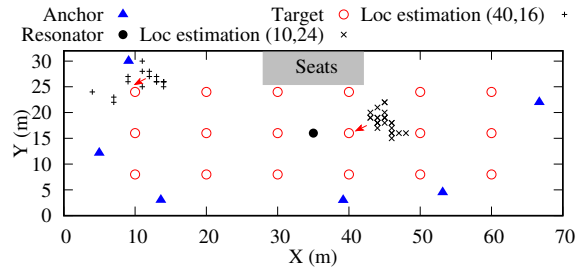Fig. 7. The meeting room deployment.

Fig. 8. The corridor deployment.

(a) Panorama of the sports hall (seen from the seats).

(b) The layout of the sports hall deployment.

Fig. 9. The sports hall deployment. The crosses are the localization results for the two target positions marked by arrows.

anchor signal processing, and data communications with the back-end server. The second type is based on LimeSDR [1] and Raspberry Pi 4B single-board computer. LimeSDR is about 10x cheaper than USRP N210. Most performance evaluation experiments in this paper are conducted using USRP-based anchors. In Section 6.2, we conduct experiments to compare the USRP-based and LimeSDR-based ILLOC systems.

Back-end server. Our back-end server is a workstation computer equipped with a Quadro RTX 6000 GPU. We use CuPy [42], a GPU-accelerated scientific computing library, to speed up the DPS cross-correlation computation. It takes about 0.11 s to compute the cross-correlation between two 2-chirp-long DPS sequences.

6 DEPLOYMENTS AND EVALUATION

6.1 Deployments and Experiment Methodology

6.1.1 Deployments. We deploy ILLOC in four environments.

Meeting room: To validate our DPS and JIT designs, we deploy a small-scale testbed in a meeting room. As shown in Fig. 7, the two anchors are placed at almost the same position; the target node and the resonator are also placed at almost the same position. Under this setting, the target node's groundtruth TDoA to the two anchors is zero. We use this deployment to investigate several issues: (1) impacts of various configurations, (2) performance of JIT synchronization, and (3) feasibility of using low-cost SDRs.

Corridor: We deploy a testbed in a $55 \times 2.3\text{m}^2$ corridor as shown in Fig. 8. Two anchors are deployed at the two ends of the corridor, respectively. The distance between them is 48 m. The resonator is placed at the mid point of the corridor, i.e., 24 m from each anchor. We carry the target node to visit seven positions in the corridor, with equal separation between two adjacent positions of 6 m. This corridor deployment is for evaluating ILLOC's 1D localization performance in long and narrow indoor environments.

(a) View of the plaza.
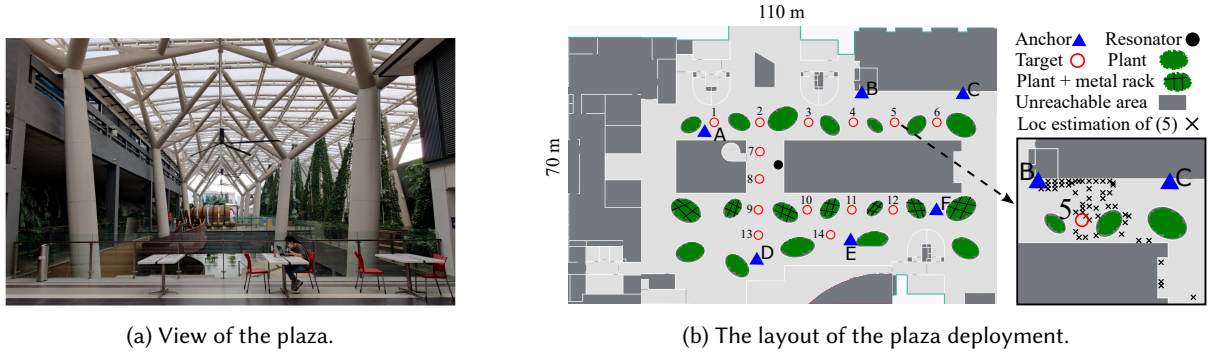
(b) The layout of the plaza deployment.

Fig. 10. The indoor plaza deployment. The crosses in the call-out figure are the localization results for position 5.

Table 4. LOS (✓) and NLOS (✗) paths in indoor plaza. 62% paths are NLOS. (R: resonator)

	1	2	3	4	5	6	7	8	9	10	11	12	13	14	R
A	✓	✗	✗	✗	✗	✗	✓	✓	✓	✓	✗	✗	✓	✓	✗
B	✓	✗	✓	✓	✗	✗	✓	✗	✗	✗	✗	✗	✗	✗	✓
C	✗	✗	✓	✗	✓	✓	✗	✗	✗	✗	✓	✗	✗	✗	✗
D	✗	✓	✗	✗	✗	✗	✓	✓	✓	✓	✗	✗	✓	✗	✓
E	✗	✗	✗	✓	✓	✗	✗	✓	✗	✓	✓	✓	✓	✓	✗
F	✗	✗	✗	✓	✓	✓	✗	✗	✗	✗	✗	✗	✗	✗	✗

Sports hall: We deploy a testbed in a sports hall sized $70 \times 32\,\mathrm{m}^2$, with ceiling about $15\,\mathrm{m}$ to $21\,\mathrm{m}$ high, as shown in Fig. 9a. Note that there are movable auditorium seats in the hall. These seats may form a barrier of the LoRa signal propagation in the hall. Fig. 9b illustrates the setup of the testbed in the hall. Six anchors, represented by blue triangles, are deployed near the edges of the hall to facilitate power supply access. The resonator, represented by the black solid dot, is placed at the center of the hall. We evenly divide the hall space into grids and carry the target node to each grid point that is represented by a red circle in Fig. 9b. We conduct experiments at a total of $6 \times 3 = 18$ target positions. The separations between two adjacent grid points in the X and Y dimensions are $10\,\mathrm{m}$ and $8\,\mathrm{m}$, respectively. We use this sports hall deployment to evaluate ILLOC's 2D localization performance.

Indoor plaza: We deploy a testbed in an indoor plaza sized $110 \times 70\,\mathrm{m}^2$, as shown in Fig. 10. The environment has extensive NLOS propagation due to the concrete pillars, bushes (green clusters in Fig. 10b), and plants climbing on large metal racks (green clusters with meshes in Fig. 10b). Six anchors are scattered inside and connected to wall power outlets. The resonator is placed at the center of the plaza. We carry the target node to 14 positions in the plaza. In Fig. 10b, unreachable areas are indicated by grey blocks. According to our on-site investigation of the LOS condition at each target node position to the anchors, all the 14 target positions and the resonator position have merely 1 to 3 LOS paths to the anchors. Table 4 shows the LOS condition. In summary, 62% paths are NLOS. We use this plaza deployment to evaluate ILLOC's localization performance in complex indoor environments with extensive NLOS propagation.

6.1.2 Evaluation Metrics. We use the following three evaluation metrics. (1) **TDoA error** is the difference between the estimated TDoA and the groundtruth TDoA, from the target node to two anchors. This metric characterizes the accuracy of our TDoA estimation method based on DPS and JIT. As the highest resolution of the estimation is one I/Q sample internal, we report TDoA errors in terms of the number of I/Q samples. (2)
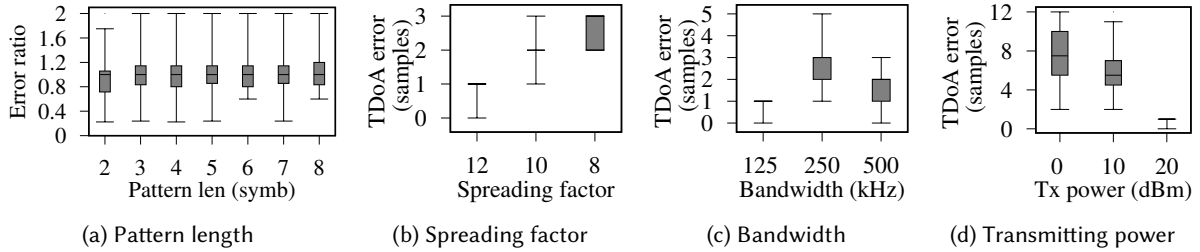
Fig. 11. Impact of various LoRaWAN and ILLOC configurations on the performance of TDoA estimation. (Whiskers of boxplots represent the 5th and 95th percentiles throughout this paper.)

Localization error is the absolute error between the estimated position and the ground truth position of the target node. This metric characterizes the localization accuracy of ILLOC that incorporates the outlier exclusion strategies. (3) **One-shot success rate** is the ratio of the one-shot successes given by Algorithm 1 to the total number of localization trials. This rate characterizes the availability of ILLOC.

6.2 Experiment Results in Meeting Room

6.2.1 Impacts of Various Configurations. We evaluate the impacts of various configurations of LoRaWAN radio and ILLOC, including spreading factor (SF), bandwidth (BW), transmitting power, and pattern length for correlation maximization. Coding rate is another LoRaWAN configuration related to the forward error correction for payload. As the DPS scheme is irrelevant to the data coding, the coding rate configuration does not affect ILLOC's performance. In this subsection, if not specifically mentioned, we by default set SF = 12, BW = 125 kHz, 20 dBm transmitting power, and the pattern length to be two symbols for the resonator/target node.

Impact of pattern length: We investigate the impact of the pattern length setting on the performance of DPS correlation maximization. We use one symbol length as the unit length in the benchmark and compute the TDoA errors with pattern lengths from one to eight preamble symbols. Fig. 11a shows the ratio of the TDoA error under a pattern length setting to that under 1-symbol pattern length. Results show that pattern lengths from one to eight symbols have similar performance, while the setting of two preamble symbols is slightly better than the other settings, with a mean error ratio of 0.975. Therefore, ILLOC chooses the setting of two preamble symbols.

Impact of SF: SF makes the trade-off between data rate and robustness to noises. From Section 2, the symbol time increases exponentially with SF. Intuitively, the robustness of ILLOC's DPS correlation maximization increases with the symbol time. Thus, larger SF settings are beneficial to ILLOC. In our experiments, we set SF to be 12, 10, and 8. The results in Fig. 11b confirm that higher SF settings lead to more accurate ranging.

Impact of BW: From Section 2, the symbol time decreases with BW. As all LoRaWAN's BW options (i.e., 125 kHz, 250 kHz, and 500 kHz) are narrow, the CSS signals under all BW options are smooth in time domain. Therefore, the BW's effect on the symbol time mainly affects ILLOC's performance. We conduct experiments with the three BW options. From Fig. 11c, the narrowest BW of 125 kHz achieves smaller TDoA errors.

Impact of transmitting power: We set the transmitting power of the target node to be 0 dBm, 10 dBm, and 20 dBm. Fig. 11d shows that ILLOC's ranging accuracy increases with the transmitting power. This is consistent with the intuition that the higher signal-to-noise ratios due to higher transmitting powers are beneficial.

6.2.2 Performance of JIT Synchronization. First, we evaluate the impact of the JIT synchronization on TDoA estimation. Since the groundtruth TDoA in this deployment is zero, the TDoA estimated by ILLOC is the TDoA error. From our measurement, the resonator has an average response delay of 58 ms in transmitting the sync
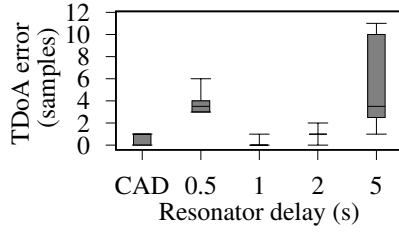
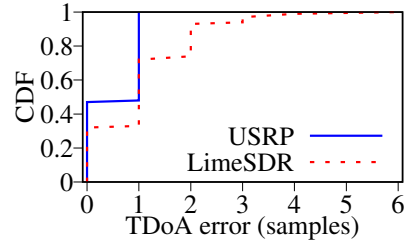Fig. 12. TDoA error with different resonator delays.

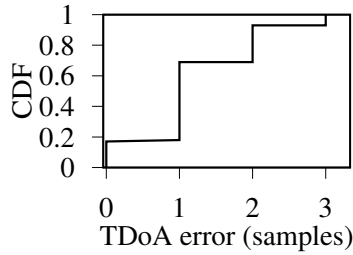
Fig. 13. TDoA error CDFs using different SDRs.
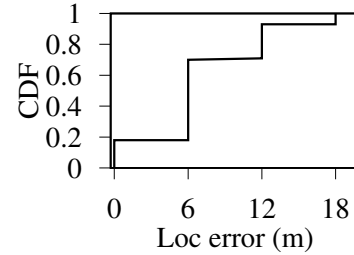

Fig. 14. Corridor TDoA error CDF.

Fig. 15. Corridor localization error CDF.

frame as a response to the target frame. This delay is longer than the CAD duration of 33 ms, because it also includes other delays such as OS delay. However, the anchors' new clock skews during the 58 ms can be still ignored. The box plot labeled "CAD" in Fig. 12 shows the distribution of the TDoA errors in repeated experiments. Specifically, the errors are binary – either zero or one sample interval – and 47% are zero.

Then, we stretch the evaluation by artificially introducing extra response delays of the resonator. The extra delays are 0.5, 1, 2, and 5 seconds. The corresponding TDoA error distributions are shown as box plots in Fig. 12. When the extra delay is 0.5 seconds, the TDoA error can reach six sample intervals. With 5 seconds extra response delay, the TDoA error is up to 11 sample intervals. The large TDoA errors are caused by the anchors' new and distinct clock skews developed during the resonator's longer response delays. With one or two seconds extra delays, the TDoA errors are smaller than those with 0.5 seconds extra delays. This is because that the anchors' clock drift rates fluctuate. Nevertheless, shorter response delays are beneficial to dealing with the anchors' clock drifts. The results suggest that the resonator is important for accurate and stable localization.

6.2.3 Using Low-cost SDRs. Fig. 13 shows the CDFs of the TDoA errors produced by the USRP-based and LimeSDR-based ILLOC systems that adopt the same SDR sampling rate of 25 Msps. The LimeSDR-based ILLOC produces larger TDoA errors. The median and mean TDoA errors of the LimeSDR-based ILLOC are one and 1.08 sample intervals, while those of the USRP-based ILLOC are one and 0.53 sample intervals, respectively. The better performance of USRP may be due to its more stable internal oscillator. Though LimeSDR yields slightly lower performance, some more LimeSDR-based anchors can be deployed to attain the 2D localization accuracy achieved by fewer USRP-based anchors.

6.3 Experiment Results in Corridor

We perform 40 localization trials at each of the seven target positions shown in Fig. 8. Fig. 14 shows the CDF of TDoA errors. The median TDoA error is one sample interval. The average TDoA error is 1.2 sample intervals.
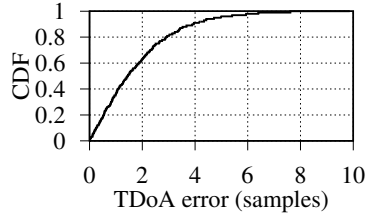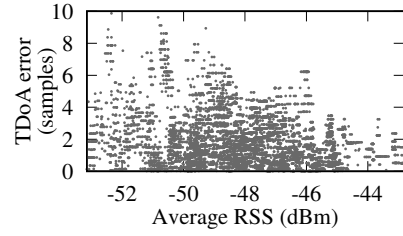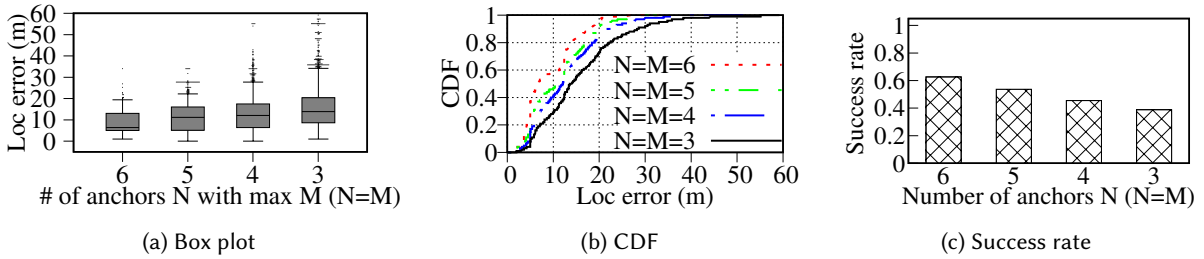
Fig. 16. Sports hall TDoA error CDF.

Fig. 17. Impact of RSS on TDoA estimation accuracy. Average RSS indicates the mean RSS of the 4 node-anchor pairs among 2 nodes and 2 anchors.

(a) Box plot

(b) CDF

(c) Success rate

Fig. 18. ILLOC's localization error and one-shot success rate when all N sensors available are used (i.e., $M = N$).

About 93% TDoA errors are within two sample intervals. Fig. 15 shows the CDF of the 1D localization errors. The median and average 1D localization errors are 6 m and 7.14 m. About 96% 1D localization errors are within the RF propagation distance within one sample interval (i.e., 12 m). The one-shot success rate is 98.57%. Only four out of the 280 localization trials yield one-shot failures. The above results show that ILLOC can perform 1D localization in long halls like a corridor.

6.4 Experiment Results in Sports Hall

In the sports hall deployment, we evaluate the TDoA errors, assess the localization errors and one-shot success rates with different numbers of available anchors (N) and different sizes of anchor subsets (M) used by Algorithm 1. Lastly, we evaluate the effectiveness of Algorithm 1 in improving the one-shot success rate.

6.4.1 Overall TDoA Errors. We perform 25 localization trials at each of the 18 target positions shown in Fig. 9b. Fig. 16 shows the TDoA error CDF. The median TDoA error is 1.44 sample intervals. Compared with the corridor deployment, the median TDoA error in sports hall is larger, possibly due to stronger multi-path effect.

6.4.2 Impact of RSS. We investigate the impact of RSS on TDoA error. Since each TDoA measurement involves two nodes (target node and resonator) and two anchors, we use the average RSS of the four node-anchor pairs to characterize the signal reception quality for the TDoA process. Fig. 17 shows the scatter plot of TDoA error versus average RSS. We can see that when the average RSS is lower, the TDoA errors are scattered in a larger range. This is because, when the RSS is lower, the random effect of the channel noises is more pronounced.

6.4.3 Impact of N and M. We conduct three sets of experiments. First, we vary N and set $M = N$. Fig. 18 shows the box plot and CDF of the localization errors, as well as the one-shot success rate. For $N = 6, 5, 4, 3$, the median localization errors are 6.40 m, 11.18 m, 12.04 m, and 13.89 m, and the one-shot success rates are 62.58%, 53.67%,
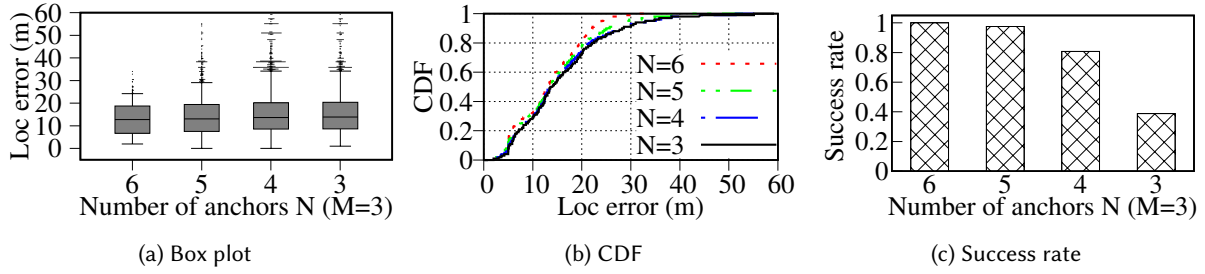
(a) Box plot

(b) CDF

(c) Success rate

Fig. 19. ILLOC's localization error and one-shot success rate when $M = 3$ and N varies from 3 to 6.
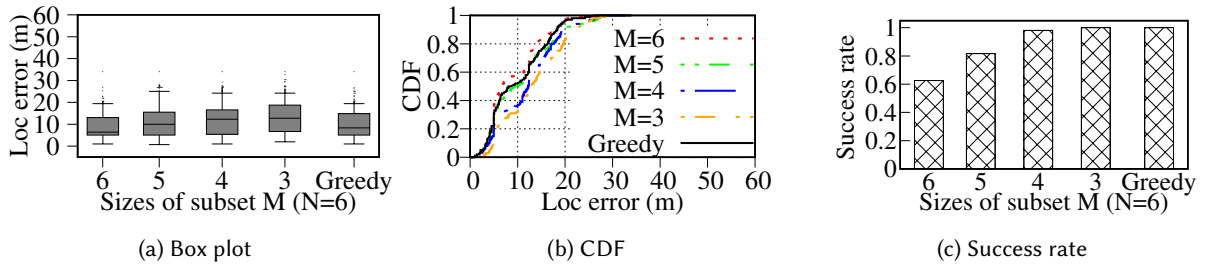

(a) Box plot

(b) CDF

(c) Success rate

Fig. 20. ILLOC's localization error and one-shot success rate when $N = 6$ and M varies from 3 to 6, or the greedy algorithm is used to dynamically configure M.

45.47%, and 38.78%, respectively. Note that only the localization errors of the successful localization trials are counted for computing the median. We can see that both the localization accuracy and one-shot success rate increase with N. This observation is consistent with intuition. Second, we fix $M = 3$ and vary N. Fig. 19a shows the results. The median localization errors for $N = 6, 5, 4, 3$ are 12.75 m, 13.04 m, 13.68 m, and 13.89 m, respectively. Thus, compared with the previous set of experiments, the localization accuracy degrades. However, by comparing Fig. 18c and Fig. 19c, we can see the one-shot success rate is improved by introducing the subset fusion mechanism discussed in Section 4.4. Third, we fix $N = 6$ and vary M from 6 to 3. Fig. 20 shows the results. With $M = 6, 5, 4, 3$, the median localization errors are 6.40 m, 10.01 m, 12.27 m, and 12.75 m, respectively, and the one-shot success rate increases from 62.58% to 100%.

From the results in Fig. 18, Fig. 19, and Fig. 20, we have the following two observations. First, the localization accuracy increases with the total number of anchors N. Second, the subset fusion mechanism may degrade localization accuracy but improve the one-shot success rate. Specifically, the localization accuracy increases with M but the one-shot success rate decreases with M.

6.4.4 Effectiveness of Greedy Anchor Subset Fusion. Given the above two observations, the greedy anchor subset fusion algorithm in Algorithm 1 will exhibit its advantage of preserving accuracy and improving the one-shot success rate at the same time. As shown in Fig. 20, it achieves a median localization error of 8.36 m and an average localization error of 10.06 m. Fig. 20b reveals that 55% of the cases have sub-10 m localization errors, and 93% of the cases have sub-20 m localization errors. While it maintains the localization accuracy of using six anchors (as shown in Fig. 20a), it achieves 100% one-shot success rate (as shown in Fig. 20c). These results clearly show the effectiveness of the greedy anchor subset fusion algorithm. The crosses in Fig. 9b show the localization results for two target positions marked by arrows.
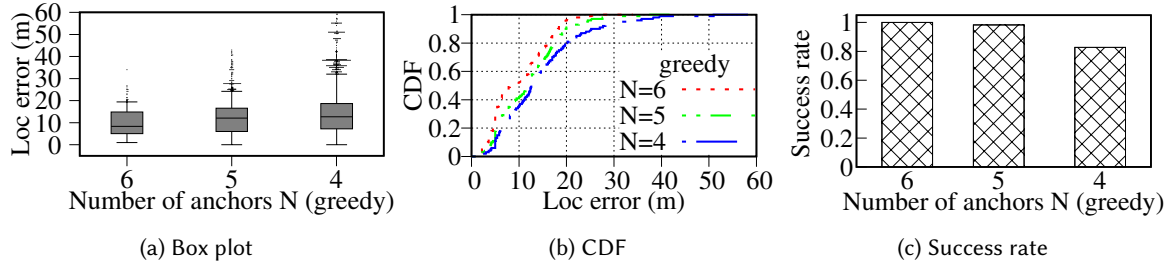
Fig. 21. ILLOC's localization error and one-shot success rate with the greedy algorithm when N varies from 6 to 4.
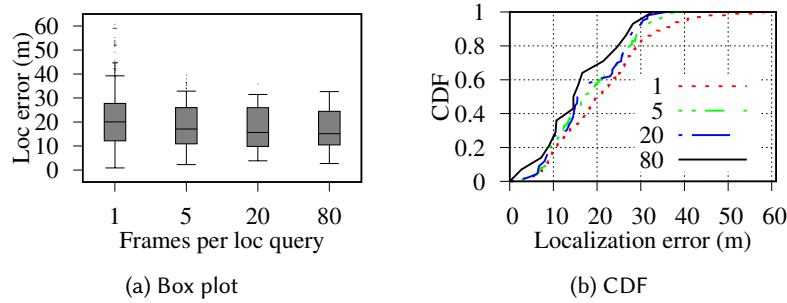

Fig. 22. ILLOC's localization errors in the indoor plaza with different numbers of frames per localization query.
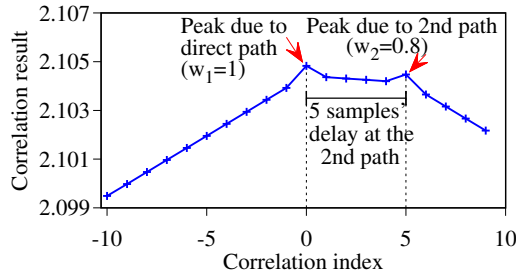
We also test the greedy anchor subset fusion with different total numbers of anchors N. The results are shown in Fig. 21. When N drops to 5 and 4, the median localization errors are 10.19 m and 12.05 m, and the one-shot success rate drop to 98.27% and 82.79% respectively. The results show that more available anchors in total can provide both higher localization accuracy and one-shot success rate, as the subset fusion is more diverse.

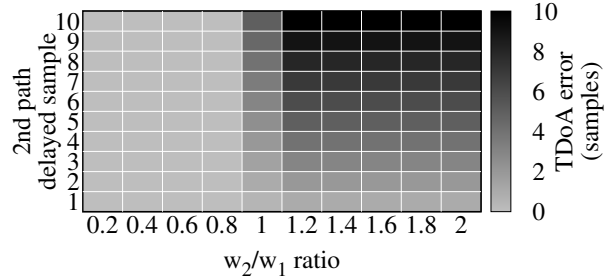## 6.5 Experiment Results in Indoor Plaza

To cope with the extensive NLOS propagation in the indoor plaza, for a target node, we fuse its localization results for multiple uplink frames to generate a single localization result. Specifically, the greedy anchor subset fusion algorithm over 6 anchors is used to estimate the target node's position for each uplink frame. The geometric median of the estimated positions for multiple frames is yielded as the final estimate of the target node position. Note that OwLL [8] also fuses 80 to 120 frames in different frequencies within both TV whitespace and ISM bands for each localization query. Fig. 22 shows the distributions of the localization errors. For one-shot localization (one frame per localization query), the median and average localization errors are 20.07 m and 21.08 m, with 100% one-shot success rate. With a frame fusion scheme, when 5, 20, 80 consecutive frames are fused to generate the final estimate, ILLOC can reduce the median errors to 17.08 m, 15.61 m, and 15.16 m, respectively. This accuracy level is similar to OwLL's 15.7 m median error for NLOS locations [8] in an outdoor environment. We expect that, in such a barrier-rich hall-size area, mounting the anchors and resonators on the ceiling may improve the LOS condition and thus ILLOC's localization performance.

6.6 A Simulation on the Impact of Multi-Path Effect

Multi-path effect is a key challenge for wireless indoor localization. While all our experiment results encompass the impact of multi-path effect, we conduct a barebone simulation study that considers two paths only to obtain

(a) Example of the two correlation peaks under the two-path model ($w_1 = 1$, $w_2 = 0.8$).

(b) TDoA error versus w_2/w_1 and propagation delay over the secondary path.

Fig. 23. Impact of a secondary signal propagation path on ILLOC's TDoA estimation.

insights into the impact of multi-path effect on ILLOC. Note that modeling the real scenarios with countless paths is challenging. Specifically, consider two anchors A and B that are perfectly synchronized and equidistant from a target node X. Assume there is no multi-path effect between A and X. Between B and X, we simulate a two-path model consisting of a direct path and a secondary path that is longer. Let w_1 and w_2 denote the powers of the received signals traveling through the direct and secondary paths. We fix $w_1 = 1$ and vary w_2 from 0.2 to 2. We also vary the difference between the arrival times of the signals traveling through the two paths. Fig. 23a shows the cross-correlation trace when $w_1 = 1$, $w_2 = 0.8$, and the difference of the arrival times is 5 sample points. We can see two cross-correlation peaks corresponding to the two paths. As the peak of the direct path is higher than that of the secondary path, the TDoA error is zero. Fig. 23b shows the TDoA errors versus w_2/w_1 and the difference of the arrival times over the two paths. We can see that when $w_2/w_1 < 1$, the secondary path generates no impact on the TDoA estimation; when $w_2/w_1 > 1$, the TDoA error equals the difference of the arrival times. This simulation result suggests that, under the general multi-path case, if the aggregate of the signals over the NLOS paths surpasses the signal over the LOS path in energy, we may have additional TDoA errors beyond that caused by random noises. However, in real environments, NLOS paths usually have larger attenuation factors due to their longer travel distances, reflections, scattering, and diffraction. In addition, the large granularity of 12 m per sample for SDR operating at 25 Msps reduces the impact of the NLOS paths that are longer than the LOS path by up to 12 m.

7 DISCUSSIONS

In this section, we discuss several issues based on the evaluation results obtained in Section 6.

10m-level localization accuracy: From our extensive evaluation results, ILLOC achieves 10m-level localization accuracy. Intuitively, ILLOC hits the accuracy limit of device localization based on the standard LoRa signal sampled at 25 Msps, because an alignment error of a single sample point during the cross-correlation maximization leads to 12 m error. The 10m-level localization accuracy suggests that most TDoA errors are zero and one sample. A high ranging resolution (i.e., 12 m in ILLOC) is the basis for achieving similar ranging/localization errors. ILLOC addresses the narrowband and clock skew challenges to fully exploit this basis. Note that 25 Msps is the highest stable sampling rate that USRP N210 and LimeSDR can achieve. Using SDRs operating at higher sampling rates may bring localization accuracy improvement, which is left for future study. The 10m-level localization accuracy can be useful in a number of applications as discussed in Section 1. While our results provide insights into understanding the feasibility and performance limit of in-hall localization under the main constraint of LoRa's narrowband nature, ILLOC is useful when the operator of an already deployed LoRaWAN wishes to

roughly track the locations of the end devices. If precise locations of end devices are required, LoRaWAN is not the best choice for engineering a localization system; other solutions (e.g., UWB) and retrofits to the end devices will be needed.

Additional communication overhead: To address the anchors' clock skews, ILLOC uses a resonator to transmit a sync frame immediately after the target frame is detected. This doubles frequency spectrum usage. To mitigate this issue, ILLOC can command the resonator to transmit the sync frame only when localization is needed. In addition, ILLOC can selectively perform localization for a single end device or a set of end devices. Specifically, ILLOC can defer the decision of whether to transmit a sync frame until the end device ID is decoded from the target frame. Our evaluation results in Fig. 12 show that the JIT synchronization can tolerate up to two seconds delay in transmitting the sync frame.

Compatibility with concurrent uplink frames: ILLOC can handle concurrent uplink frames in different frequency channels. As LoRa's CAD feature can only monitor one frequency channel at a time, ILLOC can deploy multiple resonators listening to all the used frequency channels. The resonators should use the same SF and same sync channel, and follow a CAD-based carrier sense multiple access (CSMA) protocol (e.g., [15]) to avoid sync frame collisions. This design ensures that every target frame is followed by a corresponding sync frame. Alternatively, ILLOC can deploy an SDR to monitor all frequency channels and transmit a single sync frame corresponding to all concurrent target frames. In this alternative design, the sync frame is shared by all concurrent target frames. LoRaWAN also supports concurrent uplink frames in the same frequency channel but different SF channels. The DPS scheme cannot address such same-frequency concurrent frames and ILLOC will render a one-shot failure. However, as ILLOC can estimate an end device's location using any of its uplink frames without frequency collision, ILLOC's serviceability degradation for the end device can be acceptable, unless the LoRaWAN is very dense such that the frequency collisions are frequent. Nevertheless, handling frequency-collided frames is an open issue to ILLOC, OwLL [8], and Seirios [36], and interesting for further research.

Anchor deployment: The placement of anchor and resonator is a one-time effort and environment-dependent. In this paper, we select the anchor positions based on the locations of available power outlets, while aiming to scatter the anchors and minimize signal blockage. We place the resonator near the center of the indoor space, expecting to achieve good received signal quality at all the anchors. If possible, placing the anchors at open and high places, which is also suggested by Semtech's outdoor solution [50], may provide more LOS and thus improve ILLOC's performance. Besides, it is also recommended to consider the dilution of precision (DOP) [32] when deploying the anchors (and resonators in ILLOC) in multilateration systems. Existing works [23, 24, 47] have studied the DOP minimization problem for anchor placement. We leave the detailed study of optimizing ILLOC's anchor and resonator placement to future work.

Deployment cost: In Table 1, ILLOC, OwLL [8], and Seirios [36] require SDR-based anchors, while other systems use commodity LoRaWAN gateways. While the research-oriented USRP SDR is expensive, this paper also shows the feasibility of using LimeSDRs that cost about 300 US$ per unit. With the development and increasing availability, SDR hardware cost has been decreasing and is down to 88 US$ per unit now [2]. Thus, the deployment cost of ILLOC can be similar to the solutions based on commodity gateways that cost about 135 US$ per unit [16].

8 CONCLUSION

This paper presents ILLOC, a system for unobtrusively localizing LoRaWAN end devices in a hall-size indoor space with standard uplink frames from the device. ILLOC's TDoA-based localization approach exploits LoRaWAN's multiple frequency channels and Channel Activity Detection to enable a just-in-time synchronization scheme for anchors, in which a resonator end device transmits a time reference signal once upon detecting an uplink frame for localization. Based on LoRa's CSS modulation, we design the DPS scheme to remove the unknown anchor phase terms and accumulate the CSS pattern in time for precise TDoA estimation. In the localization phase,

we use a greedy anchor subset fusion strategy to maintain localization accuracy while improving the one-shot success rate. We implement an ILLOC prototype system with two types of SDRs and off-the-shelf LoRaWAN end devices. In a 55 m long corridor deployed with two anchors, the median localization error is 6 m. In a $70 \times 32\,\text{m}^2$ sports hall deployed with six anchors, the median localization error is 8.36 m. In a $110 \times 70\,\text{m}^2$ indoor plaza with extensive NLOS propagation, ILLOC with six anchors and frame fusion achieves a median error of about 15 m with frame fusion.

ACKNOWLEDGMENTS

REFERENCES

[1] 2020. *LimeSDR*. https://limemicro.com/products/boards/limesdr/
[2] 2021. HackRF 1MHz to 6GHz SDR Platform. https://www.aliexpress.com/item/32809842995.html.
[3] 2022. *gr-lora*. https://github.com/rpp0/gr-lora
[4] Michiel Aernouts, Rafael Berkvens, Koen Van Vlaenderen, and Maarten Weyn. 2018. Sigfox and LoRaWAN datasets for fingerprint localization in large urban and rural areas. *Data* 3, 2 (2018), 13.
[5] Roshan Ayyalasomayajula, Aditya Arun, Chenfeng Wu, Sanatan Sharma, Abhishek Rajkumar Sethi, Deepak Vasisht, and Dinesh Bharadia. 2020. Deep learning based wireless localization for indoor navigation. In *Proceedings of the 26th Annual International Conference on Mobile Computing and Networking*. 1–14.
[6] Roshan Ayyalasomayajula, Deepak Vasisht, and Dinesh Bharadia. 2018. BLoc: CSI-based accurate localization for BLE tags. In *Proceedings of the 14th International Conference on emerging Networking EXperiments and Technologies*. 126–138.
[7] Wafae Bakkali, Michel Kieffer, Massinissa Lalam, and Thierry Lestable. 2017. Kalman filter-based localization for Internet of Things LoRaWAN™ end points. In *2017 IEEE 28th Annual International Symposium on Personal, Indoor, and Mobile Radio Communications (PIMRC)*. IEEE, 1–6.
[8] Atul Bansal, Akshay Gadre, Vaibhav Singh, Anthony Rowe, Bob Iannucci, and Swarun Kumar. 2021. OwLL: Accurate LoRa Localization using the TV Whitespaces. In *Proceedings of the 20th International Conference on Information Processing in Sensor Networks*. 148–162.
[9] Valentina Bianchi, Paolo Ciampolini, and Ilaria De Munari. 2018. RSSI-based indoor localization and identification for ZigBee wireless sensor networks in smart homes. *IEEE Transactions on Instrumentation and Measurement* 68, 2 (2018), 566–575.
[10] James Blackman. 2020. *Bemis mixes Sigfox and BLE for indoor and outdoor tracking of smart shopping carts*. https://enterpriseiotinsights.com/20200622/channels/news/bemis-mixes-sigfox-and-ble-for-indoor-and-outdoor-tracking-of-smart-shopping-carts
[11] Dongyao Chen, Kang G Shin, Yurong Jiang, and Kyu-Han Kim. 2017. Locating and tracking ble beacons with smartphones. In *Proceedings of the 13th International Conference on emerging Networking EXperiments and Technologies*. 263–275.
[12] Pablo Corbalán, Gian Pietro Picco, and Sameera Palipana. 2019. Chorus: UWB concurrent transmissions for GPS-like passive localization of countless targets. In *Proceedings of the 18th International Conference on Information Processing in Sensor Networks*. IEEE, 133–144.
[13] Manuel Eichelberger, Kevin Luchsinger, Simon Tanner, and Roger Wattenhofer. 2017. Indoor localization with aircraft signals. In *Proceedings of the 15th ACM Conference on Embedded Network Sensor Systems*. 1–14.
[14] Bernat Carbonés Fargas and Martin Nordal Petersen. 2017. GPS-free geolocation using LoRa in low-power WANs. In *2017 Global Internet of Things Summit (Giots)*. IEEE, 1–6.
[15] Amalinda Gamage, Jansen Christian Liando, Chaojie Gu, Rui Tan, and Mo Li. 2020. LMAC: Efficient carrier-sense multiple access for lora. In *Proceedings of the 26th Annual International Conference on Mobile Computing and Networking*. 1–13.
[16] IMST GmbH. 2021. iC880A - LoRa Concentrator. https://shop.imst.de/wireless-modules/lora-products/8/ic880a-spi-lorawan-concentrator-868-mhz.
[17] Wei Gong and Jiangchuan Liu. 2018. SiFi: Pushing the limit of time-based WiFi localization using a single commodity access point. *Proceedings of the ACM on Interactive, Mobile, Wearable and Ubiquitous Technologies* 2, 1 (2018), 1–21.
[18] Bernhard Großwindhager, Michael Stocker, Michael Rath, Carlo Alberto Boano, and Kay Römer. 2019. SnapLoc: An ultra-fast UWB-based indoor localization system for an unlimited number of tags. In *Proceedings of the 18th ACM/IEEE International Conference on Information Processing in Sensor Networks*. 61–72.
[19] Chaojie Gu, Linshan Jiang, Rui Tan, Mo Li, and Jun Huang. 2021. Attack-aware synchronization-free data timestamping in lorawan. *ACM Transactions on Sensor Networks (TOSN)* 18, 1 (2021), 1–31.

[20] Zhe He, You Li, Ling Pei, and Kyle O'Keefe. 2018. Enhanced Gaussian process-based localization using a low power wide area network. *IEEE Communications Letters* 23, 1 (2018), 164–167.

[21] Bashima Islam, Md Tamzeed Islam, Jasleen Kaur, and Shahriar Nirjon. 2019. Lorain: Making a case for lora in indoor localization. In *2019 IEEE International Conference on Pervasive Computing and Communications Workshops (PerCom Workshops)*. IEEE, 423–426.

[22] Chengkun Jiang, Yuan He, Songzhen Yang, Junchen Guo, and Yunhao Liu. 2019. 3D-OmniTrack: 3D tracking with COTS RFID systems. In *Proceedings of the 18th ACM/IEEE International Conference on Information Processing in Sensor Networks*. 25–36.

[23] Damien B Jourdan and Nicholas Roy. 2008. Optimal sensor placement for agent localization. *ACM Transactions on Sensor Networks (TOSN)* 4, 3 (2008), 1–40.

[24] Nicolaj Kirchhof. 2013. Optimal placement of multiple sensors for localization applications. In *International Conference on Indoor Positioning and Indoor Navigation*. IEEE, 1–10.

[25] Manikanta Kotaru, Kiran Joshi, Dinesh Bharadia, and Sachin Katti. 2015. Spotfi: Decimeter level localization using wifi. In *Proceedings of the 2015 ACM Conference on Special Interest Group on Data Communication*. 269–282.

[26] Swarun Kumar, Stephanie Gil, Dina Katabi, and Daniela Rus. 2014. Accurate indoor localization with zero start-up cost. In *Proceedings of the 20th annual international conference on Mobile computing and networking*. 483–494.

[27] Swarun Kumar, Ezzeldin Hamed, Dina Katabi, and Li Erran Li. 2014. LTE radio analytics made easy and accessible. *ACM SIGCOMM Computer Communication Review* 44, 4 (2014), 211–222.

[28] Ye-Sheng Kuo, Pat Pannuto, Ko-Jen Hsiao, and Prabal Dutta. 2014. Luxapose: Indoor positioning with mobile phones and visible light. In *Proceedings of the 20th annual international conference on Mobile computing and networking*. 447–458.

[29] Myeongcheol Kwak, Youngmong Park, Junyoung Kim, Jinyoung Han, and Taekyoung Kwon. 2018. An energy-efficient and lightweight indoor localization system for Internet-of-Things (IoT) environments. *Proceedings of the ACM on Interactive, Mobile, Wearable and Ubiquitous Technologies* 2, 1 (2018), 1–28.

[30] Hussein Kwasme and Sabit Ekin. 2019. RSSI-based localization using LoRaWAN technology. *IEEE Access* 7 (2019), 99856–99866.

[31] Ka-Ho Lam, Chi-Chung Cheung, and Wah-Ching Lee. 2019. RSSI-Based LoRa Localization Systems for Large-Scale Indoor and Outdoor Environments. *IEEE Transactions on Vehicular Technology* 68, 12 (2019), 11778–11791.

[32] Richard B Langley et al. 1999. Dilution of precision. *GPS world* 10, 5 (1999), 52–59.

[33] Patrick Lazik, Niranjini Rajagopal, Oliver Shih, Bruno Sinopoli, and Anthony Rowe. 2015. ALPS: A bluetooth and ultrasound platform for mapping and localization. In *Proceedings of the 13th ACM conference on Embedded Networked Sensor Systems*. 73–84.

[34] Liqun Li, Pan Hu, Chunyi Peng, Guobin Shen, and Feng Zhao. 2014. Epsilon: a visible light based positioning system. In *Proceedings of the 11th USENIX Conference on Networked Systems Design and Implementation*. 331–343.

[35] Yuxiang Lin, Wei Dong, Yi Gao, and Tao Gu. 2020. SateLoc: A Virtual Fingerprinting Approach to Outdoor LoRa Localization using Satellite Images. In *Proceedings of the 19th ACM/IEEE International Conference on Information Processing in Sensor Networks*.

[36] Jun Liu, Jiayao Gao, Sanjay Jha, and Wen Hu. 2021. Seirios: leveraging multiple channels for LoRaWAN indoor and outdoor localization. In *Proceedings of the 27th Annual International Conference on Mobile Computing and Networking*. 656–669.

[37] Inc. LoRa Alliance. 2017. LoRaWAN 1.1 Specification.

[38] Yunfei Ma, Nicholas Selby, and Fadel Adib. 2017. Minding the billions: Ultra-wideband localization for deployed rfid tags. In *Proceedings of the 23rd annual international conference on mobile computing and networking*. 248–260.

[39] Sandeep Mistry. 2022. *Arduino-LoRa*. https://github.com/sandeepmistry/arduino-LoRa

[40] Ruthwik Muppala, Abhinav Navnit, Deeksha Devendra, Eustachio Roberto Matera, Nicola Accettura, and Aftab M Hussain. 2021. Feasibility of Standalone TDoA-based Localization Using LoRaWAN. In *International Conference on Localization and GNSS*. IEEE, 1–7.

[41] Rajalakshmi Nandakumar, Vikram Iyer, and Shyamnath Gollakota. 2018. 3d localization for sub-centimeter sized devices. In *Proceedings of the 16th ACM Conference on Embedded Networked Sensor Systems*. 108–119.

[42] Ryosuke Okuta, Yuya Unno, Daisuke Nishino, Shohei Hido, and Crissman Loomis. 2017. CuPy: A NumPy-Compatible Library for NVIDIA GPU Calculations. In *NIPS Workshop*. http://learningsys.org/nips17/assets/papers/paper_16.pdf

[43] Veljo Otsason, Alex Varshavsky, Anthony LaMarca, and Eyal De Lara. 2005. Accurate GSM indoor localization. In *International conference on ubiquitous computing*. Springer, 141–158.

[44] Messaoud Ahmed Ouameur, Manouane Caza-Szoka, and Daniel Massicotte. 2020. Machine learning enabled tools and methods for indoor localization using low power wireless network. *Internet of Things* (2020), 100300.

[45] Nico Podevijn, David Plets, Jens Trogh, Luc Martens, Pieter Suanet, Kim Hendrikse, and Wout Joseph. 2018. TDoA-based outdoor positioning with tracking algorithm in a public LoRa network. *Wireless Communications and Mobile Computing* (2018).

[46] Jait Purohit, Xuyu Wang, Shiwen Mao, Xiaoyan Sun, and Chao Yang. 2020. Fingerprinting-based indoor and outdoor localization with LoRa and deep learning. In *IEEE Global Communications Conference*. IEEE, 1–6.

[47] Niranjini Rajagopal, Sindhura Chayapathy, Bruno Sinopoli, and Anthony Rowe. 2016. Beacon placement for range-based indoor localization. In *2016 international conference on indoor positioning and indoor navigation (IPIN)*. IEEE, 1–8.

[48] Hamada Rizk, Marwan Torki, and Moustafa Youssef. 2018. CellinDeep: Robust and accurate cellular-based indoor localization via deep learning. *IEEE Sensors Journal* 19, 6 (2018), 2305–2312.

[49] Hazem Sallouha, Alessandro Chiumento, and Sofie Pollin. 2017. Localization in long-range ultra narrow band IoT networks using RSSI. In *2017 IEEE International Conference on Communications (ICC)*. IEEE, 1–6.

[50] Semtech. 2021. *Locating End Devices with Semtech's LoRa Cloud™ Geolocation Service.* https://lora-developers.semtech.com/documentation/tech-papers-and-guides/locating-end-devices-with-lora-cloud/

[51] Semtech. 2021. *Semtech and DevAppSol Track Luggage Trolleys to Reduce Airport Management Cost With LoRaWAN.* https://www.semtech.com/company/press/semtechs-and-devappsol-track-luggage-trolleys-to-reduce-airport-management-cost-with-lorawan

[52] Masashi Sugano, Tomonori Kawazoe, Yoshikazu Ohta, and Masayuki Murata. 2006. Indoor Localization System using RSSI Measurement of Wireless Sensor Network based on ZigBee Standard. *Wireless and Optical Communications* (2006), 1–6.

[53] Vamsi Talla, Mehrdad Hessar, Bryce Kellogg, Ali Najafi, Joshua R Smith, and Shyamnath Gollakota. 2017. Lora backscatter: Enabling the vision of ubiquitous connectivity. *Proceedings of the ACM on Interactive, Mobile, Wearable and Ubiquitous Technologies* 1, 3 (2017), 1–24.

[54] Rui Tian, HaiBo Ye, and Li Sheng. 2020. Indoor Localization Based on the LoRa Technology. In *International Conference on Machine Learning and Intelligent Communications*. Springer, 304–319.

[55] Xinyu Tong, Fengyuan Zhu, Yang Wan, Xiaohua Tian, and Xinbing Wang. 2019. Batch localization based on OFDMA backscatter. *Proceedings of the ACM on Interactive, Mobile, Wearable and Ubiquitous Technologies* 3, 1 (2019), 1–25.

[56] Junpei Tsuji, Hidenori Kawamura, Keiji Suzuki, Takeshi Ikeda, Akio Sashima, and Koichi Kurumatani. 2010. ZigBee based indoor localization with particle filter estimation. In *2010 IEEE International Conference on Systems, Man and Cybernetics*. IEEE, 1115–1120.

[57] Deepak Vasisht, Guo Zhang, Omid Abari, Hsiao-Ming Lu, Jacob Flanz, and Dina Katabi. 2018. In-body backscatter communication and localization. In *Proceedings of the 2018 Conference of the ACM Special Interest Group on Data Communication*. 132–146.

[58] Davide Vecchia, Pablo Corbalán, Timofei Istomin, and Gian Pietro Picco. 2019. TALLA: Large-scale TDoA localization with ultra-wideband radios. In *2019 International Conference on Indoor Positioning and Indoor Navigation (IPIN)*. IEEE, 1–8.

[59] Jue Wang, Fadel Adib, Ross Knepper, Dina Katabi, and Daniela Rus. 2013. RF-compass: Robot object manipulation using RFIDs. In *Proceedings of the 19th annual International Conference on Mobile Computing and Networking*. 3–14.

[60] Jue Wang and Dina Katabi. 2013. Dude, where's my card? RFID positioning that works with multipath and non-line of sight. In *Proceedings of the ACM SIGCOMM 2013 conference on SIGCOMM*. 51–62.

[61] Jiang Xiao, Zimu Zhou, Youwen Yi, and Lionel M Ni. 2016. A survey on wireless indoor localization from the device perspective. *ACM Computing Surveys (CSUR)* 49, 2 (2016), 1–31.

[62] Bo Xie, Guang Tan, and Tian He. 2015. Spinlight: A high accuracy and robust light positioning system for indoor applications. In *Proceedings of the 13th ACM Conference on Embedded Networked Sensor Systems*. 211–223.

[63] Pengjin Xie, Lingkun Li, Jiliang Wang, and Yunhao Liu. 2020. LiTag: localization and posture estimation with passive visible light tags. In *Proceedings of the 18th Conference on Embedded Networked Sensor Systems*. 123–135.

[64] Jie Xiong, Karthikeyan Sundaresan, and Kyle Jamieson. 2015. Tonetrack: Leveraging frequency-agile radios for time-based indoor wireless localization. In *Proceedings of the 21st Annual International Conference on Mobile Computing and Networking*. 537–549.

[65] Huatao Xu, Dong Wang, Run Zhao, and Qian Zhang. 2019. AdaRF: Adaptive RFID-based indoor localization using deep learning enhanced holography. *Proceedings of the ACM on Interactive, Mobile, Wearable and Ubiquitous Technologies* 3, 3 (2019), 1–22.

[66] Xuehan Ye, Shuo Huang, Yongcai Wang, Wenping Chen, and Deying Li. 2019. Unsupervised localization by learning transition model. *Proceedings of the ACM on Interactive, Mobile, Wearable and Ubiquitous Technologies* 3, 2 (2019), 1–23.

[67] Faheem Zafari, Athanasios Gkelias, and Kin K Leung. 2019. A survey of indoor localization systems and technologies. *IEEE Communications Surveys & Tutorials* 21, 3 (2019), 2568–2599.

[68] Chi Zhang and Xinyu Zhang. 2017. Pulsar: Towards ubiquitous visible light localization. In *Proceedings of the 23rd Annual International Conference on Mobile Computing and Networking*. 208–221.

[69] Fusang Zhang, Zhaoxin Chang, Kai Niu, Jie Xiong, Beihong Jin, Qin Lv, and Daqing Zhang. 2020. Exploring lora for long-range through-wall sensing. *Proceedings of the ACM on Interactive, Mobile, Wearable and Ubiquitous Technologies* 4, 2 (2020), 1–27.

[70] Fusang Zhang, Zhaoxin Chang, Jie Xiong, Rong Zheng, Junqi Ma, Kai Niu, Beihong Jin, and Daqing Zhang. 2021. Unlocking the beamforming potential of lora for long-range multi-target respiration sensing. *Proceedings of the ACM on Interactive, Mobile, Wearable and Ubiquitous Technologies* 5, 2 (2021), 1–25.

[71] Hongxu Zhu, Kim-Fung Tsang, Yucheng Liu, Yang Wei, Hao Wang, Chung Kit Wu, and Hao Ran Chi. 2020. Extreme RSS based Indoor Localization for LoRaWAN with Boundary Autocorrelation. *IEEE Transactions on Industrial Informatics* 17, 7 (2020), 4458–4468.